OPTICAL SURFACE PLASMONS IN SEMICONDUCTORS

by

Xiaoou Mao

Submitted in partial fulfilment of the requirements
for the degree of Master of Applied Science

at

Dalhousie University
Halifax, Nova Scotia
August 2012

© Copyright by Xiaoou Mao, 2012

DALHOUSIE UNIVERSITY

DEPARTMENT OF ELECTRICAL AND COMPUTER ENGINEERING

The undersigned hereby certify that they have read and recommend to the Faculty of Graduate Studies for acceptance a thesis entitled "OPTICAL SURFACE PLASMONS IN SEMICONDUCTORS" by Xiaoou Mao in partial fulfilment of the requirements for the degree of Master of Applied Science.

Date: 22nd August, 2012

Supervisor: _________________________________

Readers: _________________________________

____

DALHOUSIE UNIVERSITY

DATE: 22nd August, 2012

AUTHOR: Xiaoou Mao

TITLE: OPTICAL SURFACE PLASMONS IN SEMICONDUCTORS

DEPARTMENT OR SCHOOL: Department of Electrical and Computer Engineering

DEGREE: MASc CONVOCATION: October YEAR: 2012

Permission is herewith granted to Dalhousie University to circulate and to have copied for non-commercial purposes, at its discretion, the above title upon the request of individuals or institutions. I understand that my thesis will be electronically available to the public.

The author reserves other publication rights, and neither the thesis nor extensive extracts from it may be printed or otherwise reproduced without the author's written permission.

The author attests that permission has been obtained for the use of any copyrighted material appearing in the thesis (other than the brief excerpts requiring only proper acknowledgement in scholarly writing), and that all such use is clearly acknowledged.

____

Signature of Author

To my parents Jun Mao and Jie Gao

Table of Contents

LIST OF TABLES vii
LIST OF FIGURES viii
ABSTRACT x
LIST OF ABBREVIATIONS USED xi
ACKNOWLEDGEMENTS xii
CHAPTER 1 1
INTRODUCTION 1
1.1 Surface Plasmon Polaritons (SPPs) 1
1.1.1 History of SPPs 1
1.1.2 Applications 2
1.1.3 Motivation and Objective 5
1.2 Contributions 6
1.3 Organization of the Thesis 7
CHAPTER 2 8
BACKGROUND THEORY 8
2.1 Definition of Surface Plasmon Polaritons 8
2.2 SPPs at Metal/Dielectric Interface 9
2.2.1 Maxwell's Equations 9
2.2.2 Drude Model 10
2.2.3 Derivation of the Dispersion Relation of SPPs 11
2.3 Excitation of SPPs 19
2.3.1 Prism Coupling 19
2.3.2 Grating Coupling 21
2.4 Summary 24
CHAPTER 3 25
SEMICONDUCTOR SPPs 25
3.1 Features of SPPs at Semiconductor/Dielectric Interface 26
3.1.1 Lower Frequency of SPPs 26
3.1.2 Active Control of Semiconductor based SPPs 26
3.2 Theoretical Treatment and the New Unique Solution 28

3.3 Design and Data Selection 34
3.3.1 Properties of Heavily Doped Silicon 35
3.3.2 Effective mass 35
3.3.3 Relaxation Time 40
CHAPTER 4 42
RESULTS and DISCUSSIONS 42
4.1 The Effect of Damping on ω_3 43
4.2 System Design and Analysis of the Result 45
4.3 Error Analysis 51
CHAPTER 5 53
CONCLUSION and FUTURE WORK 53
5.1 Conclusion and Contribution 53
5.2 Future work 54
BIBLIOGRAPHY 55

LIST OF TABLES

Table 1 Value of ω_3 for sample free electron densities and corresponding wavelength 47

Table 2 Values of original ω_3 and ω_3' which were calculated from reducing the effective mass by 5 per cent 51

LIST OF FIGURES

Figure 1.1 The main idea of SPPs biosensor's design ... 3
Figure 1.2 SPPs affinity biosensors[14] ... 4
Figure 1.3 SPPs sensors implementation (a) Prism couplers, (b) grating couplers and (c) waveguide couplers[14] ... 4

Figure 2.1 Definition of a planar waveguide geometry. The waves propagate along the x-direction in a Cartesian coordinate system. [7] ... 12
Figure 2.2 Geometry for SPP propagation at a single interface between a metal and a dielectric. [7] ... 14
Figure 2.3 The charges and the electromagnetic field of SPPs propagating on a surface in the x direction are shown schematically ... 15
Figure 2.4 Dispersion relation of SPP for an metal/air structure ... 17
Figure 2.5 Experimental arrangements Left: Otto configuration. Right: Kretschmann configuration. L: laser, D: detector, M: metal layer.[14] ... 20
Figure 2.6 The Prism coupling method: Dispersion relation of SPPS for a prism/metal/air system $\varepsilon 2 = 1$, c: light line in vacuum, $c/\varepsilon 0$: light line in the medium ε_0 ... 20
Figure 2.7 Phase-matching of light to SPPs using a grating.[7] ... 22
Figure 2.8 SEM image of two microhole arrays with period 760 nm and hole diameter 250 nm separated by 30 μm used for sourcing (right array) and probing (left array) of SPPs ... 22
Figure 2.9 (a) Near-field optical image of the pattern presented in Fig. 2.8 when the illuminating laser is focused on the small array on the right with the electric field polarised in the *x*-direction ... 23

Figure 3.1 Semiconductor/Dielectric Structure to excite SPP ... 25
Figure 3.2 Classical dispersion curve for a surface plasmon at metal/air interface draw from equation (3.7).. ... 31
Figure 3.3 Dispersion characteristics of semiconductor/dielectric interface.. ... 32
Figure 3.4 Carrier concentration dependence of free electron effective mass (m^*) and carrier relaxation time (τ).[27] ... 36
Figure 3.5 Effective mass of free carriers as a function of carrier concentration ... 39
Figure 3.6 Density dependence of the electron effective mass of electrons for T = 300K (solid curve) and T = 3000K (dash-dot curve) ... 39
Figure 3.7 Carrier concentration dependence of carrier relaxation time (τ).[27] ... 40
Figure 3.8 Relaxation time of free carriers as a function of carrier concentration. ×[27], ● homogeneous profile, ○ inhomogeneous profile.[30] ... 41

Figure 4.1 Structure used to excite SPPs ... 42

Figure 4.2 SPPs dispersion characteristics at Si/SiO_2 interface with electron density of Si equal to $2.5*10^{27}$ m^{-3}, (a) ω_3 ignore loss from damping equation (3.9) and (b) ω_3 contain loss from damping equation (3.12).....44
Figure 4.3 SPPs dispersion characteristics at Si/SiO_2 interface with electron density of Si equal to $1*10^{27}$ m^{-3} and ω_3 = 0.5631 eV. 45
Figure 4.4 SPPs dispersion characteristics at Si/SiO_2 interface with electron density of Si equal to $1.5*10^{27}$ m^{-3} and ω_3 = 0.6661 eV. 46
Figure 4.5 SPPs dispersion characteristics at Si/SiO_2 interface with electron density of Si equal to $2*10^{27}$ m^{-3} and ω_3 = 0.7476 eV. 46
Figure 4.6 SPPs dispersion characteristics at Si/SiO_2 interface with electron density of Si equal to $3*10^{27}$ m^{-3} and ω_3 = 0.8803 eV. 47
Figure 4.7 Plot of the regression equation and sample points 49
Figure 4.8 SPPs dispersion relation at free electron density $2.35*10^{27}m^{-3}$, ω_3 and $\omega_3^{'}$ are calculated for m^* = $0.5080m_0$ and m^* = $0.50737m_0$ which are interpolated from Fig 3.6 and calculated from regression equation(4.1). 50

ABSTRACT

A theoretical treatment is presented of a plasmonic interaction at an interface between a semiconductor and a dielectric, as opposed to the more traditional configuration whereby a metal/dielectric interface is investigated. Our work is to show that structures using semiconductors instead of metal to excite surface plasmon can support not only terahertz frequencies plasmons but also optical frequency (around 10^{15}Hz) plasmons.

LIST OF ABBREVIATIONS USED

c	Speed of light
e	Electron charge
D	Dielectric displacement
E	Electric field
H	Magnetic field
B	Magnetic induction or magnetic flux density
P	Electric dipole moment
J_{ext}	External current density
ρ_{ext}	External charge density
N	Free carrier density
n	Refractive index
ε	Material permittivity
ε_s	Permittivity of semiconductor
ε_d	Permittivity of dielectric
ε_0	Permittivity of vacuum
μ_0	Vacuum permeability
m_0	Effective mass of electron
$\boldsymbol{\lambda}$	Wavelength
ω	Angular frequency
ω_p	Plasma frequency
ω_{sp}	Surface Plasmon Frequency
k_0	Wave vector of propagating wave in vacuum
β	Propagation constant of the traveling waves
k_1	Wave vector in material 1
k_2	Wave vector in material 2
θ	Angle of incident light
a	Grating constant
γ	Damping constant
τ	Relaxation time

ACKNOWLEDGEMENTS

I would like to express my sincere gratitude to my supervisor Dr. Michael Cada for his helpful guidance, constant patience and encouragement throughout my graduate study. The deep insight and extensive knowledge were very helpful to me. And also, I am appreciated to have Dr. Zhizhang Chen and Dr. Guy C. Kember on my supervisory committee.

I am also very grateful to my friends in Photonics Applications Lab for their selfless support. Special thanks to Franklin Che for many fruitful discussions and constructive advice.

Also, I want to thank my best friends in Halifax for their help and advice about my life here and about my future career. And thanks to people who make me more mature than before.

Especially, I would like to give my endless thanks and love to my parents for their consistent love and support for both my studies and in my personal life.

CHAPTER 1

INTRODUCTION

In this chapter, the overview of the thesis is presented. Also the motivation of the design and objective are included.

1.1 Surface Plasmon Polaritons (SPPs)

1.1.1 History of SPPs

Surface Plasmon Polaritons (SPPs) are electromagnetic surface waves propagating between a dielectric and a conductor, evanescently confined in the perpendicular direction. They arise via the coupling of the electromagnetic fields to oscillations of the metal's electron plasma. SPPs can propagate along the surface of a metal until energy is lost either via absorption in the metal or radiation into free-space.

The history of the study of SPPs can be traced back to 1902, while Robert W. Wood first observed the abnormal intensity drops in spectra produced when visible light reflects at metallic gratings in the visible domain [1]. Thirty nine years later, U .J .Fano explained this phenomenon by connecting it with the excitation of electromagnetic field on the metal/air interface [2] in 1941. In 1957, Rufus Ritchie recorded loss phenomena associated with interactions taking place at metallic surfaces via the diffraction of electron beams at thin metallic foils [3] which is seen as the first theoretical description of surface Plasmon. And in 1968, it linked with the original work on diffraction gratings in the optical domain [4]. At the same time, two groups of researcher Kretschmann and Raether [5] and Otto [6] successfully excited SPPs on

metal surface with visible light using prism coupler and a unified description of all these phenomena in the form SPPs was established.

Since then the research in this field has been so firmly grounded in the visible region of the spectrum, that several rediscoveries in the microwave and the terahertz domain took place at the turn of the 21st century, closing the circle with the original work from 100 years earlier. [7]

1.1.2 Applications

Surface Plasmon Polariton (SPPs) propagate along the metal/dielectric interface, evanescently confined in the perpendicular direction. The wavelength of SPPs is very small which makes it possible to confine the energy in a nanometer scale. This character of SPPs is attracting increasing attention as a potential type of information carrier for a highly integrated photonic device to be developed in the futre. Also, this promising technology might close the size gap between electronic and optical devices. Current research has predicted and proved that SPPs has broad future prospects in many application areas include nanophotonics technology, data storage, microscopy, solar cell and biosensor etc. We are going to give several examples of SPPs application and their advantages in the following paragraphs.

- SPPs Integrated Circuit

  The capacity of electrical devices is limited as an information carrier which can not fully content the explosive increasing requirement of speed and capacity in the information processing system. As we all know, optical devices have the characteristics of high speed and wide bandwidth compared to electronic devices and the photon computer is expected to be the next generation computer. Yet the size of the optical devices is around micro-meter which is close to the wavelength of light and the losses increases with the deduction of the size. This fact makes the interconnection between optical

devices (micrometer scale) and electronic devices (nanometer scale) impossible. SPPs give us a perfect solution which takes advantage of both high speed and compact size. Surface Plasmon Polaritons built a bridge between optical and electronic devices for us.

- SPPs Biosensor

SPPs are evanescently bound to the metal surface and they are sensitive to dielectric perturbations at the surface. Consequently, metals can be used to sense the binding of molecules to the surface in a technique called Surface Plasmon Polariton sensing. [8] Attenuated Total Reflection, also known as the Kretschmann geometry, is the most common method for SPP. The Figure 1.1 shows the main idea of SPPs biosensor's design. Majority of SPPs sensors are based on the interrogation of the plasmonic wave propagation at metal/dielectric interface.

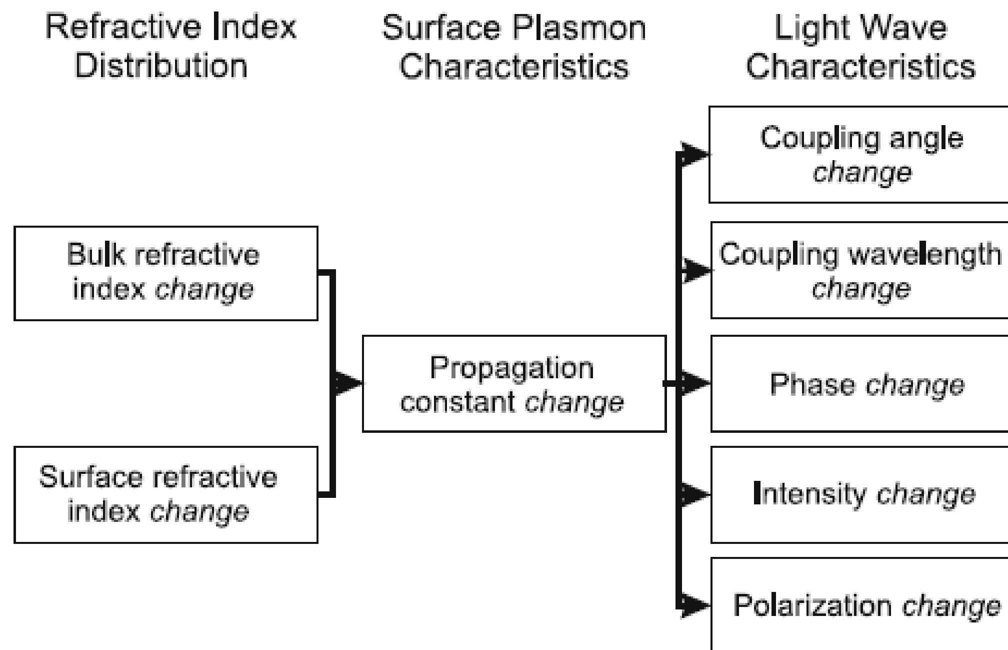

Figure 1.1 The main idea of SPPs biosensor's design

Fig 1.2 shows the structure of SPPs affinity biosensors which can incorporate biorecognition elements that are able to interact with a selected analyte.

Analyte molecules in solution bind to the molecular recognition elements increasing the refractive index (Δn) on the metal superstrate that changes a propagation constant of surface plasmons. And Fig 1.3 shows three SPP sensors implementation: (a) Prism couplers, (b) grating couplers and (c) waveguide couplers. The main idea is the same but the way of exciting SPPs is different. We will introduce the excitation of SPPs in the Chapter 2 later.

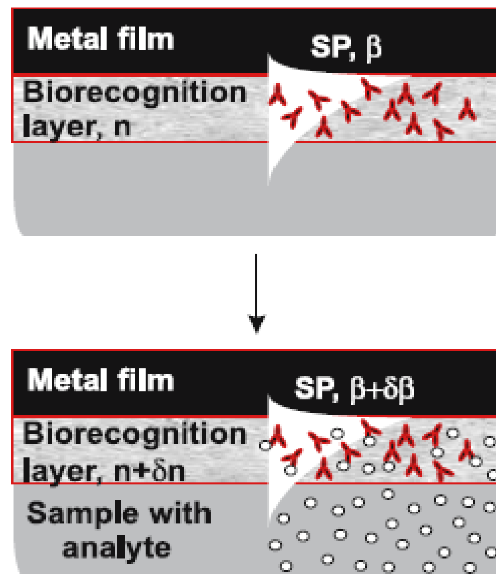

Figure 1.2 SPPs affinity biosensors[14]

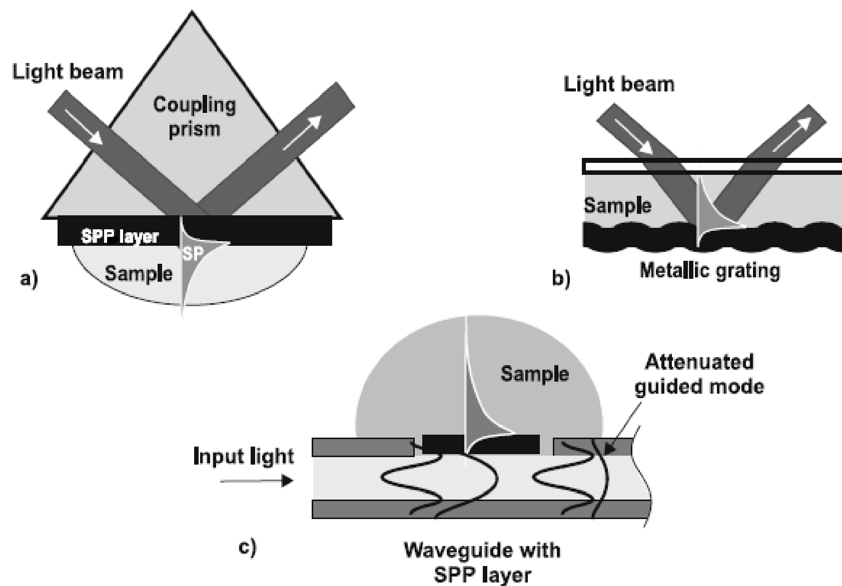

Figure 1.3 SPPs sensors implementation (a) Prism couplers, (b) grating couplers and (c) waveguide couplers[14]

- Nanolithography and Subwavelength Imaging

  Surface plasmons propagation can be controlled by metal nanostructures in nanometer scale. This achieves the function of the shrink of the optical wavelength and recaptures evanescent waves that are lost in conventional imaging, which is the origin of the diffraction limit. Therefore, it is natural to apply nanostructure metals to nanolithography and subwavelength imaging. There is great research potential for using metal nanostructures to achieve extreme subwavelength focusing [9].

1.1.3 Motivation and Objective

Owing to the unique properties of Surface Plasmon Polaritons(SPPs) in diverse electronic and photonic applications, research on SPPs wave is promising and attracting vast numbers of researchers including both physicist and engineers. At the same time, semiconductors — especially Silicon — is widely used in electronic devices. As we mentioned, the use of SPPs is a potential solution to close the gap of the size between electronic and optical devices. Thus the SPPs excited at semiconductor/dielectric interface attracted our attention. Most of the effort has been concentrated on investigating SPPs in the visible domain on metal surfaces; however, not only metals support electron plasma oscillations, semiconductors can also support SPPs with a resulting plasma frequency typically in the terahertz domain. Our original objective is to find out the properties of SPPs based on semiconductor/dielectric structure when the semiconductor is heavily doped.

1.2 Contributions

By re-deriving the dispersion relation of SPPs based on the classical method using Maxwell equations as the core, we find out a new solution which is only possible to exist in the semiconductor/dielectric structure while two other solutions of dispersion relation remain the same with the metal/dielectric structure. This is due to the fact the permittivity of semiconductor is larger than metal's. We will explain this mathematically in the Chapter 3. The new solution is like standing waves with group velocity equal to zero in theory. The physical meaning of it is not clear until we do the experiment to observe but first the mathematical approach is needed. Thus we focused on the Silicon/Silicon Dioxide structure and fulfilled the requirement of exciting the SPPs in optical frequency by heavily doped Silicon. To calculate the frequency of the well know solution and the new solution of SPPs, the properties of Silicon under an extremely high free carrier density are studied including effective mass of electrons, permittivity and relaxation time. We proved that the wavelength of the new solution of SPPs can be excited by the commonly used optical communication wavelengths 1.55 μm which may lead to an application in a communication system or data transfer.

1.3 Organization of the Thesis

The Thesis is organized as follows. Chapter 2 describes some of the general theories underlying SPPs, including the physical and mathematical explanation to SPPs. The derivation of SPPs dispersion relation use Maxwell equations on metal/dielectric interface. After that, the excitation of SPPs using different structures is explained. Chapter 3 introduced the features of SPPs at semiconductor/dielectric interface and then the derivation of SPPs dispersion relation is given, which shows the process of finding the new solution. At the end of Chapter 3 the optical properties of heavily doped Silicon are discussed. In Chapter 4, the results calculated from the data taken from Chapter 3 will be shown and discussed. And an error analysis for the design will be given. Finally, Chapter 5 concludes the whole thesis and make some suggestions for future work.

CHAPTER 2

BACKGROUND THEORY

2.1 Definition of Surface Plasmon Polaritons

At the beginning, we will introduce the meaning of Plasmon and Polariton separately for a better understanding of those terms. The Plasmon is a quasiparticle resulting from the quantization of plasma oscillations just as photons is quantization of light. Polariton refers to a wave of polarizations, positive and negative charges in a row. Plasmons couple with photons to create another quasiparticle called plasma Polariton. Thus Surface Plasmons are those Plasmons that are confined to surfaces and that interact strongly with light resulting in a Polariton. It can be roughly defined as the combination of a particle and its influence on the local environment.

2.2 SPPs at Metal/Dielectric Interface

2.2.1 Maxwell's Equations

As mentioned above, Surface Plasmon Polaritons are electromagnetic surface waves that arise via the coupling of the electromagnetic fields (optical wave) to oscillations of the conductor's electron plasma. And a neutral gas of charged particles is called plasma. Metals and doped semiconductors can be treated as plasmas because they contain equal numbers of fixe*d* positive ions and free electrons. The free electrons experience no restoring forces when they interact with electromagnetic waves. [10]

As a starting point, the following which comes from the well-known Maxwell's equations of macroscopic electromagnetism,

$$\nabla \cdot \boldsymbol{D} = \rho_{ext} \tag{2.1 a}$$

$$\nabla \cdot \boldsymbol{B} = 0 \tag{2.1 b}$$

$$\nabla \times \boldsymbol{E} = -\frac{\partial \boldsymbol{B}}{\partial t} \tag{2.1 c}$$

$$\nabla \times \boldsymbol{H} = J_{ext} + \frac{\partial \boldsymbol{D}}{\partial t}. \tag{2.1 a}$$

The relationship among ***D*** (the dielectric displacement), ***E*** (the electric field), ***H*** (the magnetic field), ***B*** (the magnetic induction or magnetic flux density) and the external charge and current densities ρ_{ext} and J_{ext} is thus presented. Furthermore, they can be written in the form:

$$\boldsymbol{D} = \varepsilon_0 \boldsymbol{E} + \boldsymbol{P} \tag{2.2 a}$$

$$\boldsymbol{H} = \frac{1}{\mu_0}\boldsymbol{B} - \boldsymbol{M}, \tag{2.2 b}$$

where ε_0 and $\mu_0$are the electric permittivity and Magnetic permeability of vacuum respectively. ***P*** describes the electric dipole moment. The process uses the Maxwell equation for the derivations of dielectric function and SPPs dispersion relation will be discussed in section 2.2.3.

2.2.2 Drude Model

We consider only the effects of the free electrons and apply the Drude model for the free-electron gas. As a starting point, one can apply the Drude model for the free-electron gas and write a simple equation of motion for an electron of the plasma sea in metal subjected to an external electric field $\boldsymbol{E}$:

$$\ddot{\boldsymbol{x}} + m\gamma\dot{\boldsymbol{x}} = -e\boldsymbol{E}. \tag{2.3}$$

Here x is the displacement of plasma caused by the electric field while m and e are the charge and effective mass of the free electrons. Assuming harmonic time dependence $\boldsymbol{E}(t) = E_0 e^{-i\omega t}$ of the driving electric field, we can find a particular solution of this equation describing the oscillation of the electron as $\boldsymbol{x}(t) = x_0 e^{-i\omega t}$. The complex amplitude x_0 incorporates any phase shifts between driving field and response via:

$$\boldsymbol{x}(t) = \frac{e}{m_0(\omega^2 + i\gamma\omega)}\boldsymbol{E}(t). \tag{2.4}$$

The displaced electrons contribute to the macroscopic polarization$\boldsymbol{P} = -Ne\boldsymbol{x}$, where N is the free carrier density. Thus insert $\boldsymbol{P} = -Ne\boldsymbol{x}$ into equation 2.2:

$$\boldsymbol{P} = -\frac{Ne^2}{m_0(\omega^2 + i\gamma\omega)}\boldsymbol{E}. \tag{2.5}$$

Insertion of this expression for P into equation (2.2a) yields:

$$\boldsymbol{D} = \varepsilon_0\left(1 - \frac{\omega_p^2}{\omega^2 + i\gamma\omega}\right)\boldsymbol{E}, \tag{2.6}$$

where $\omega_p = \sqrt{\frac{Ne^2}{\varepsilon_0 m^*}}$ is the plasma frequency of the free electron gas where N is the electron density, e is the charge of the electron, m^* is the effective mass of the electron and ε_0 is the permittivity of free-space. Therefore we get the dielectric function for an ideal free-electron metal:

$$\varepsilon(\omega) = 1 - \frac{\omega_p^2}{\omega^2 + i\gamma\omega}. \tag{2.7}$$

For a more general case, residual polarization due to the positive background of the ion cores can be described by adding the term $P_\infty = \varepsilon_0(\varepsilon_\infty - 1)\boldsymbol{E}$ to equation (2.2 a). And we can rewrite the dielectric function of free electron gas:

$$\varepsilon(\omega) = \varepsilon_\infty - \frac{\omega_p^2}{\omega^2 + i\gamma\omega}, \tag{2.8}$$

where ε_∞ is the dielectric constant at infinite frequency that usually equals to 1 for metal.

2.2.3 Derivation of the Dispersion Relation of SPPs

Dispersion relation describes the relation between wave vector and frequency which is used to study the physical properties of electromagnetic waves. To get the dispersion relation of SPPs, Maxwell's equations (2.1) is solved.

Apply Maxwell's equations (2.1) to the flat interface between a conductor and a dielectric with the condition that there be no no external charge and current densities. The curl equations (2.1c, 2.1d) can be combined to yield:

$$\nabla \times \nabla \times \boldsymbol{E} = -\mu_0 \frac{\partial^2 D}{\partial t^2}. \tag{2.9}$$

Using the mathematical identities $\nabla \times \nabla \times \boldsymbol{E} \equiv \nabla(\nabla \cdot \boldsymbol{E}) - \nabla^2 \boldsymbol{E}$ and$\nabla \cdot (\varepsilon \boldsymbol{E}) \equiv \boldsymbol{E} \cdot \nabla\varepsilon + \varepsilon\nabla \cdot \mathbf{E}$, (2.9) can be rewritten as

$$\nabla\left(-\frac{1}{\varepsilon}\boldsymbol{E} \cdot \nabla\varepsilon\right) - \nabla^2 \boldsymbol{E} = -\mu_0 \varepsilon_0 \varepsilon \frac{\partial^2 \boldsymbol{E}}{\partial t^2}. \tag{2.10}$$

For negligible variation of the dielectric constant $\varepsilon = \varepsilon(r)$ over distances on the order of one optical wavelength, (2.10) simplifies to the central equation of electromagnetic wave theory

$$\nabla^2 \boldsymbol{E} - \frac{\varepsilon}{c^2}\frac{\partial^2 \boldsymbol{E}}{\partial t^2} = 0. \tag{2.11}$$

To cast (2.11) in a form suitable for the description of confined propagating waves, we proceed in two steps. First, we assume in all generality a harmonic time dependence $\boldsymbol{E}(\boldsymbol{r}, t) = \boldsymbol{E}(\boldsymbol{r})e^{-i\omega t}$ of the electric field. Inserted into (2.11), this yields

$$\nabla^2 \boldsymbol{E} + k_0^2 \varepsilon \boldsymbol{E} = 0, \tag{2.12}$$

where $k_0 = \frac{\omega}{c}$ is the wave vector of the propagating wave in vacuum. Equation (2.12) is known as the Helmholtz equation. [11]

Next, we are going to define the propagation geometry. We consider a one-dimensional problem for simplicity, thus ε depends only on one spatial coordinate. Assume the waves propagate along the x-direction of a Cartesian coordinate system, and show no spatial variation in the perpendicular, in-plane y-direction (see Fig. 2.1); therefore $\varepsilon = \varepsilon(z)$. Applied to electromagnetic surface problems, the plane $z = 0$ coincides with the interface sustaining the propagating waves, which can now be described as $\boldsymbol{E}(x, y, z) = \boldsymbol{E}(z)e^{i\beta x}$. The complex parameter $\beta = k_x$ is called the propagation constant of the traveling waves and corresponds to the component of the wave vector in the direction of propagation. Inserting this expression into (2.12) yields the desired form of the wave equation

$$\frac{\partial^2 \boldsymbol{E}(z)}{\partial z^2} + (k_0^2 \varepsilon - \beta^2)\boldsymbol{E} = 0. \tag{2.13}$$

For an electromagnetic wave, a similar equation exists for the magnetic field $\boldsymbol{H}$.

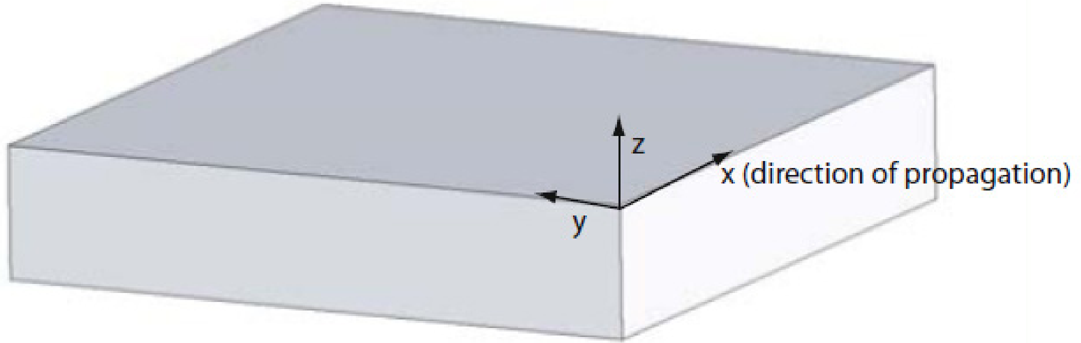

Figure 2.1 Definition of a planar waveguide geometry. The waves propagate along the x-direction in a Cartesian coordinate system. [7]

Equation (2.13) is the starting point for the general analysis of guided electromagnetic modes in waveguides, and an extended discussion of its properties and applications can be found in [12] and similar treatments of photonics and optoelectronics. In order to use the wave equation for determining the spatial field profile and dispersion of propagating waves, we now need to find explicit expressions for the different field

components of **E** and **H**. This can be achieved in a straightforward way using the curl equations (2.1c, 2.1d).

For harmonic time dependence $(\frac{\partial}{\partial t} = -i\omega)$, we arrive at the following set of coupled equations

$$\frac{\partial E_z}{\partial y} - \frac{\partial E_y}{\partial z} = i\omega\mu_0 H_x \tag{2.14a}$$

$$\frac{\partial E_x}{\partial z} - \frac{\partial E_z}{\partial x} = i\omega\mu_0 H_y \tag{2.14b}$$

$$\frac{\partial E_y}{\partial x} - \frac{\partial E_x}{\partial y} = i\omega\mu_0 H_z \tag{2.14c}$$

$$\frac{\partial H_z}{\partial y} - \frac{\partial H_y}{\partial z} = -i\omega\varepsilon_0\varepsilon E_x \tag{2.14d}$$

$$\frac{\partial H_x}{\partial z} - \frac{\partial H_z}{\partial x} = -i\omega\varepsilon_0\varepsilon E_y \tag{2.14e}$$

$$\frac{\partial H_y}{\partial x} - \frac{\partial H_y}{\partial z} = -i\omega\varepsilon_0\varepsilon E_z. \tag{2.14f}$$

For propagation along the x-direction $(\frac{\partial}{\partial x} = i\beta)$ and homogeneity in the y-direction $(\frac{\partial}{\partial y} = 0)$, this system of equation simplifies to

$$\frac{\partial E_y}{\partial z} = -i\omega\mu_0 H_x \tag{2.15a}$$

$$\frac{\partial E_x}{\partial z} - i\beta E_z = i\omega\mu_0 H_y \tag{2.15b}$$

$$i\beta E_y = i\omega\mu_0 H_z \tag{2.15c}$$

$$\frac{\partial H_y}{\partial z} = i\omega\varepsilon_0\varepsilon E_x \tag{2.15d}$$

$$\frac{\partial H_x}{\partial z} - i\beta H_z = -i\omega\varepsilon_0\varepsilon E_y \tag{2.15e}$$

$$i\beta H_y = -i\omega\varepsilon_0\varepsilon E_z. \tag{2.15f}$$

This system allows two sets of self-consistent solutions with different polarization properties of the propagating waves. They are the transverse magnetic (TM or p) modes, where only the field components E_x, E_z and H_y are nonzero and transverse electric (TE or s) modes, with only H_x, H_z and E_y being nonzero.

For TM modes, the system of governing equations (2.15) reduces to

$$E_x = -i\frac{1}{\omega\varepsilon_0\varepsilon}\frac{\partial H_y}{\partial z} \tag{2.16a}$$

$$E_z = -i\frac{1}{\omega\varepsilon_0\varepsilon}\frac{\partial H_y}{\partial z} \tag{2.16b}$$

and the wave equation for TM modes is

$$\frac{\partial^2 H_y}{\partial z^2} + (k_0^2\varepsilon - \beta^2)H_y = 0. \tag{2.16c}$$

For TE modes the corresponding equation set is

$$H_x = i\frac{1}{\omega\mu_0}\frac{\partial E_y}{\partial z} \tag{2.17a}$$

$$H_z = \frac{\beta}{\omega\mu_0}E_y \tag{2.17b}$$

with the TE wave equation

$$\frac{\partial^2 E_y}{\partial z^2} + (k_0^2\varepsilon - \beta^2)E_y = 0. \tag{2.17c}$$

Now with equations above, we can derive the description of surface plasmon polaritons on a single, flat interface (Fig. 2.2) between a dielectric, non-absorbing half space ($z > 0$) with positive real dielectric constant ε_2 and an adjacent conducting half space ($z < 0$) described via a dielectric function $\mathrm{Re}[\varepsilon_1] < 0$. As shown by the Drude model for metals before, this condition is fulfilled at frequencies below the bulk plasmon frequency ω_p. We are looking for propagating wave solutions has its maximum at the surface $z = 0$, with evanescent decay in the perpendicular z-direction. Fig 2.3 shows the surface wave of TM mode.

Figure 2.2 Geometry for SPP propagation at a single interface between a metal and a

dielectric. [7]

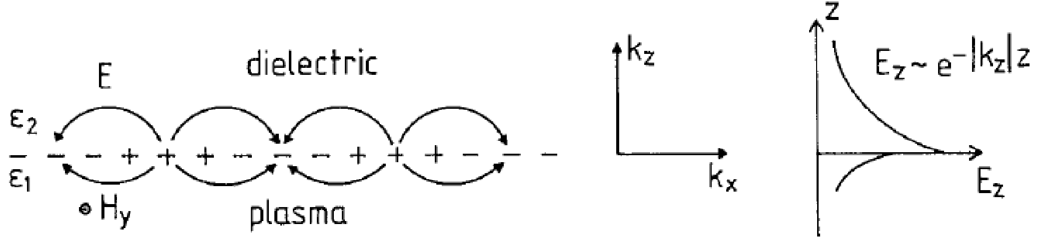

Figure 2.3 The charges and the electromagnetic field of SPPs propagating on a surface in the x direction are shown schematically. The exponential dependence of the field E_z is seen on the right. H_y shows the magnetic field in the y direction of this p-polarized wave. [13]

First, we derive the SPPs dispersion relation for TM mode. Using the equations (2.15) in both half spaces yields

$$H_y(z) = A_2 e^{i\beta x} e^{-k_2 z} \tag{2.18a}$$

$$E_x(z) = iA_2 \frac{1}{\omega\varepsilon_0\varepsilon_2} k_2 e^{i\beta x} e^{-k_2 z} \tag{2.18b}$$

$$E_z(z) = -A_2 \frac{\beta}{\omega\varepsilon_0\varepsilon_2} e^{i\beta x} e^{-k_2 z} \tag{2.18c}$$

for z > 0 and

$$H_y(z) = A_1 e^{i\beta x} e^{k_1 z} \tag{2.19a}$$

$$E_x(z) = -iA_1 \frac{1}{\omega\varepsilon_0\varepsilon_1} k_1 e^{i\beta x} e^{k_1 z} \tag{2.19b}$$

$$E_z(z) = -A_1 \frac{\beta}{\omega\varepsilon_0\varepsilon_1} e^{i\beta x} e^{k_1 z} \tag{2.19c}$$

for z < 0. $k_i = k_{z,i}$ (i=1,2) is the component of the wave vector perpendicular to the interface in the two media. Its reciprocal value, $1/|k_z|$ defines the evanescent decay length of the fields perpendicular to the interface, which quantifies the confinement of the wave. Continuity of H_y and $\varepsilon_i E_z$ at the interface requires that A_1=A_2 and

$$\frac{k_2}{k_1} = -\frac{\varepsilon_2}{\varepsilon_1}. \tag{2.20}$$

Since the wavevector parallel to the interface is conserved the following relations hold for the wavevector components

$$\beta^2 + k_1^2 = \varepsilon_1 k_0^2 \tag{2.21a}$$

$$\beta^2 + k_2^2 = \varepsilon_2 k_0^2. \quad (2.21b)$$

Here $k_0 = \omega/c$ where ω is the frequency of SPPs and c is the speed of light in vacuum. From equation (2.20), confinement to the surface demands $Re[\varepsilon_1] < 0$ if $\varepsilon_2 > 0$ - the surface waves exist only at interfaces between materials with opposite signs of the real part of their dielectric permittivities, i.e. between a conductor and an insulator.

Combining equation (2.20) and (2.21) we arrive at the central result of this section, the dispersion relation of SPPs propagating at the interface between the two half spaces

$$\beta = k_0 \sqrt{\frac{\varepsilon_1 \varepsilon_2}{\varepsilon_1 + \varepsilon_2}}. \quad (2.22)$$

This expression is valid for both real and complex ε_1.

Now we briefly analyze the possibility of TE surface modes. Using equations (2.17), the respective expressions for the field components are

$$E_y(z) = A_2 e^{i\beta x} e^{-k_2 z} \quad (2.23a)$$

$$H_x(z) = -iA_2 \frac{1}{\omega\mu_0} k_2 e^{i\beta x} e^{-k_2 z} \quad (2.23b)$$

$$H_z(z) = A_2 \frac{\beta}{\omega\mu_0} e^{i\beta x} e^{-k_2 z} \quad (2.23c)$$

for $z > 0$ and

$$E_y(z) = A_1 e^{i\beta x} e^{k_1 z} \quad (2.24a)$$

$$H_x(z) = iA_1 \frac{1}{\omega\mu_0} k_1 e^{i\beta x} e^{k_1 z} \quad (2.24b)$$

$$H_z(z) = A_1 \frac{\beta}{\omega\mu_0} e^{i\beta x} e^{k_1 z} \quad (2.24c)$$

for $z < 0$. Continuity of E_y and H_x at the interface leads to the condition

$$A_1(k_1 + k_2) = 0. \quad (2.25)$$

Since confinement to the surface requires $Re[k_1] > 0$ and $Re[k_2] > 0$, this condition is only fulfilled when $A_1 = 0$, so that also $A_2 = A_1 = 0$. Thus, no surface modes exist for TE polarization. Surface plasmon polaritons only exist for TM polarization.

Now we examine the properties of SPPs from the dispersion relation. Fig. 2.4 shows plot of equation (2.22) - dispersion relation of SPP for an air (ε_2 =1) /metal interface .

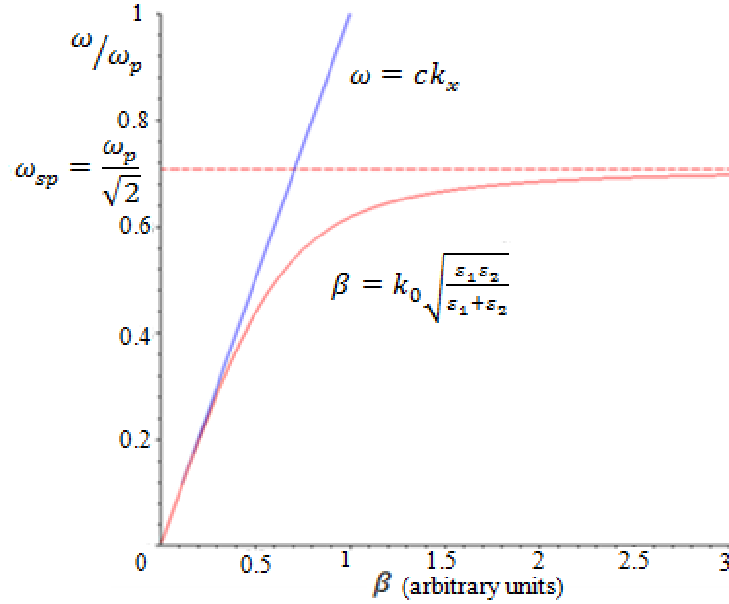

Figure 2.4 Dispersion relation of SPP at metal/air interface.

In this plot, the frequency ω is normalized to the plasma frequency ω_p. Due to the bound nature, the SPP excitations correspond to the part of the dispersion curves lying to the right of the respective light lines of air. Thus, special phase-matching techniques such as grating or prism coupling are required[7] for their excitation via three-dimensional beams, which will be discussed later.

From Fig 2.4, for small wave vectors corresponding to low (mid-infrared or lower) frequencies, the SPP propagation constant is close to k_0 at the light line, and the waves extend over many wavelengths into the dielectric space. While in the regime of large wave vector β, the frequency of the SPPs approaches the characteristic surface plasmon frequency

$$\omega_{sp} = \frac{\omega_p}{\sqrt{1+\varepsilon_2}} \ . \tag{2.26}$$

This result can be shown by inserting the free-electron dielectric function (2.7) into dispersion relation (2.22), β approaches infinity need $\varepsilon_1 = -\varepsilon_2$. Assume an ideal conductor without damping and ignore γ and we will get the equation (2.26). For the case of air ($\varepsilon_2 = 1$)/metal structure $\omega_{sp} = \frac{\omega_p}{\sqrt{2}}$. When wave vector β goes to infinity as the frequency approaches ω_{sp}, the group velocity $v_g = \frac{\partial\omega}{\partial k}$ approaches 0. The mode thus acquires electrostatic character, and is known as the surface plasmon.

2.3 Excitation of SPPs

As we mentioned, the application of photons to excite SPPs meets the difficulty that the dispersion relation always lies right from the light line ($\beta > \omega/c$). At a given photon energy $h\omega$ the wave vector $h\omega/c$ has to be increased by a Δk_x value in order to "transform" the photons into SPPs. [13] We are going to introduce two methods which are the most common techniques for SPPs excitation.

2.3.1 Prism Coupling

Surface plasmon polaritons on a flat metal/dielectric interface cannot be excited directly by light beams since $\beta > k$, where k is the wave vector of light on the dielectric side of the interface. Therefore, the projection along the interface of the momentum $k_x = k\sin\theta$ of photons impinging under an angle θ to the surface normal is always smaller than the SPPs propagation constant β, even at grazing incidence, prohibiting phase-matching.

However, phase-matching to SPPs can be achieved in a three-layer system consisting of a thin metal film sandwiched between two insulators of different dielectric constants. Light is reflected at a metal surface covered with a dielectric medium ($\varepsilon_0>1$) usually in the form of a prism (Fig 2.5). Its momentum becomes ($(h\omega/c)\sqrt{\varepsilon_0}$) instead of $h\omega/c$ and its projection on the surface (see Fig 2.6) becomes

$$k_x = \sqrt{\varepsilon_0}\frac{\omega}{c}sin\theta_0. \quad (2.27)$$

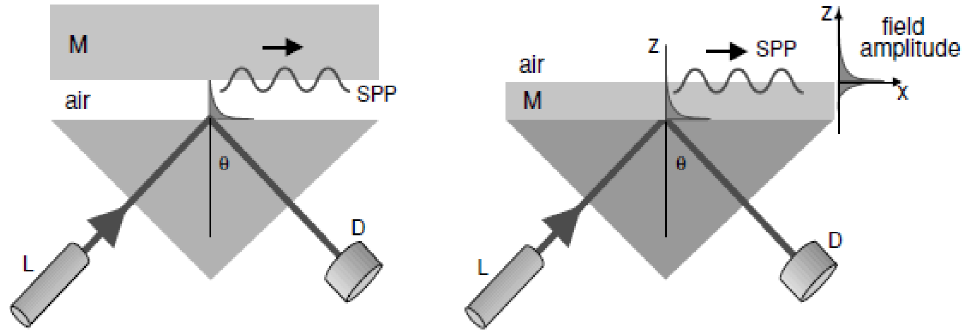

Figure 2.5 Experimental arrangements Left: Otto configuration. Right: Kretschmann configuration. L: laser, D: detector, M: metal layer.[14]

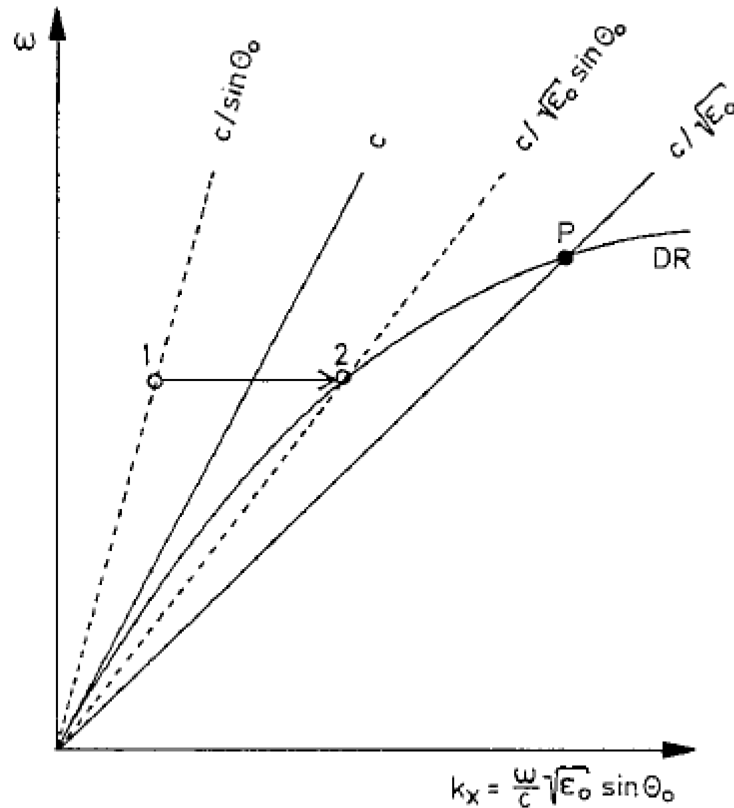

Figure 2.6 The Prism coupling method: Dispersion relation of SPPS for a prism/metal/air system $\varepsilon_2 = 1$, c: light line in vacuum, $c/\sqrt{\varepsilon_0}$: light line in the medium ε_0. Since the light line $c/\sqrt{\varepsilon_0}$ lies to the right of the dispersion relation up to a certain k_x, light can excite SPPs of frequencies ω below the crossing point P on the metal/air side. The SPPs on the interface metal/prism cannot be excited, since their dispersion relation lies to the right of $c/\sqrt{\varepsilon_0}$ because ε_0>1. [13]

The dispersion relation (2.22) for SPPs propagating on the interface $\varepsilon_2/\varepsilon_1$ (air/metal) can thus be satisfied between the lines c and $c/\sqrt{\varepsilon_0}$. Fig 2.6.

In Fig 2.5, two structures are shown: in the Otto[6] configuration, the metal surface is separated by a thin air gap. Total internal reflection takes place at the prism/air interface, exciting SPPs via tunneling to the air/metal interface; Another geometry is the Kretschmann method[5], a thin metal film is evaporated on top of a glass prism. Photons from a beam impinging from the glass side at an angle greater than the critical angle of total internal reflection tunnel through the metal film and excite SPPs at the metal/air interface.

2.3.2 Grating Coupling

An alternative way to excite SPPs is the use of a grating coupler. Here, the increase of the wavevector necessary to match the SPPs momentum is achieved by adding a reciprocal lattice vector of the grating to the free-space wavevector. This requires in principle that the metal surface is structured with the right periodicity 'a' over and extended spatial region. For the simple one-dimensional grating of grooves shown in Fig 2.7, phase matching takes place whenever the condition

$$\beta = ksin\theta \pm v\frac{2\pi}{a} \tag{2.28}$$

is fulfilled, where $v = (1,2,3\ldots)$.

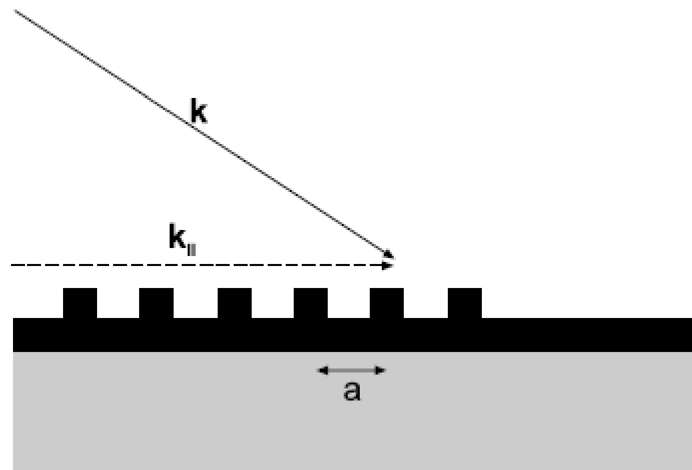

Figure 2.7 Phase-matching of light to SPPs using a grating.[7]

The reverse process can also take place: SPPs propagating along a surface modulated with a grating can couple to light and thus radiate. As an example of SPPs excitation and their decoupling via gratings, Fig 2.8 shows a scanning electron microscopy (SEM) image of a flat metal film patterned with two arrays of sub-wavelength holes [15]. In this study, the small array on the right was used for the excitation of SPPs via a normally-incident beam, while the larger array on the left decoupled the propagating SPPs to light radiation. Fig 2.9 is the near-field optical images of the excitation and detection region as well as of the propagating SPPs.

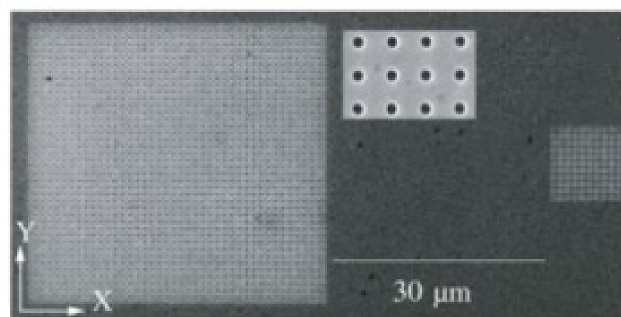

Figure 2.8 SEM image of two microhole arrays with period 760 nm and hole diameter 250 nm separated by 30 μm used for sourcing (right array) and probing (left array) of SPPs. The inset shows a close-up of individual holes. [15]

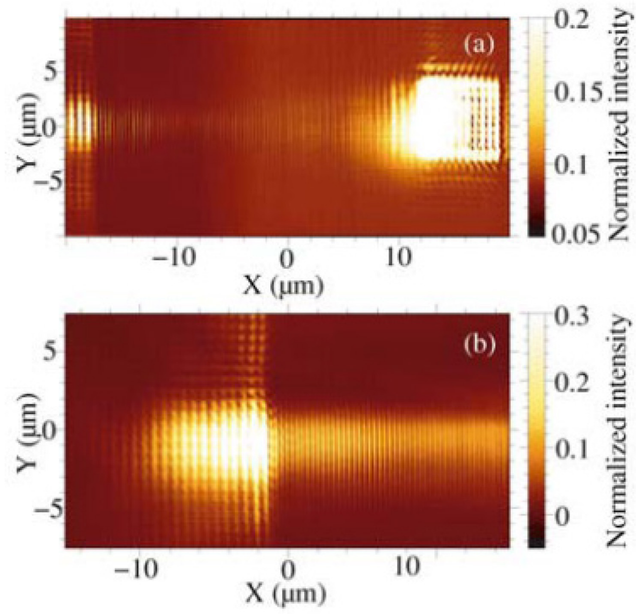

Figure 2.9 (a) Near-field optical image of the pattern presented in Fig. 2.8 when the illuminating laser is focused on the small array on the right with the electric field polarised in the *x*-direction. (b) Detail of image (a) shows propagating SPPs and the edge of the left decoupling array. A wavelength λ = 800 nm was chosen so as to coincide with the airside transmission peak in Fig. 3.7.[15]

2.4 Summary

In this Chapter, the definition of Surface plasmons polaritons is given. We started from the Maxwell wave equations to describe the fundamentals of surface plasmon polaritons at flat interfaces between metal and dielectric. Also, the excitation of SPPs using prism coupler and grating coupler are introduced.

CHAPTER 3

SEMICONDUCTOR SPPs

Surface plasmon polaritons have attracted huge attention from researchers and is a subject of intense research in recent years. Most of the effort has been concentrated on investigating SPPs in the visible and near-IR domain on metal surfaces. However, not only metals support electron plasma oscillations; semiconductors can also support SPPs, free carriers being excited either thermally or by doping, with a resulting plasma frequency typically in the terahertz(THz) domain.[16] The main idea is to treat semiconductors as metals in the conductor/dielectric structure (Fig. 3.1), SPPs excited on the semiconductor/dielectric interface have been proved possible by many researchers in THz domain based on the theory discussed before in Chapter 2.

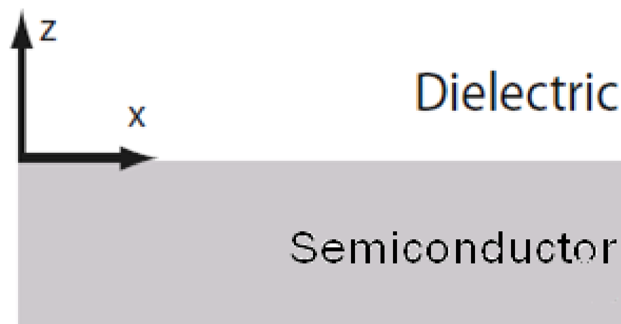

Figure 3.1 Semiconductor/Dielectric Structure to excite SPP

3.1 Features of SPPs at Semiconductor/Dielectric Interface

3.1.1 Lower Frequency of SPPs

As we mentioned, the frequency of SPPs excited on the metal/dielectric structure is in the optical and near infrared regime. Current research of SPPs excited at the semiconductor/dielectric interface is in the terahertz(THz) domain. Since semiconductor contains equal numbers of fixed positive ions and free electrons just like metal, thus the basic theories used include Maxwell's equations, Drude model, boundary and confinement conditions in deriving the wave function. Dispersion relation of SPPs at metal/dielectric interface is also available for semiconductor/dielectric structure.

Recall the SPPs frequency equation (2.26)

$$\omega_{sp} = \frac{\omega_p}{\sqrt{1+\varepsilon_2}},$$

where plasma frequency $\omega_p = \sqrt{\frac{Ne^2}{\varepsilon_0 \varepsilon_s m^*}}$, ε_s is the permittivity of undoped semiconductor. The free electron density N in metal is in the scale of 10^{28} m^{-3} while for doped semiconductor is around 10^{21} m^{-3}. Thus the plasma frequency of metal and semiconductor can be calculated from the two equations above. For metal the plasma frequency and SPPs frequency is around 10^{15}Hz which is in the 10^{12}Hz(THz) regime at the same time for semiconductors. This explained why the frequency semiconductor/dielectric SPPs is in the THz domain.

3.1.2 Active Control of Semiconductor based SPPs

A decisive advantage of semiconductors over metals is that their surface charge density can be modified by, for example chemical doping, and optical, thermal or electrical injection of free carriers. And thus plasma frequencies and SPPs properties

can be modulated within the THz frequency range. Also other properties of semiconductor (e.g. permittivity and effective mass) will change with the free carrier density and affect the SPPs frequency which we will be discussed later. Various research conducted based on the controllable feature of semiconductor has been published and is attracting intense attention.[16]-[18]

3.2 Theoretical Treatment and the New Unique Solution

In this section, we will present the theoretical treatment of SPPs excited on semiconductor/dielectric interface, as opposed to the more traditional metal/dielectric structure. We will also present a new solution, which is only possible to exist at the semiconductor/dielectric interface.[19]

At the beginning, revise the definition of plasma which is a neutral gas of charged particles. Metals and doped semiconductors can be treated as plasmas because they contain equal numbers of fixed positive ions and free electrons. [10] Our objective is to obtain dispersion characteristics of a general structure (conductor with plasma/dielectric) and study possible new effects that may exist there.

The original idea coming from Dr.Cada's previous work.[19] He's approach, which is more of an electromagnetic-field treatment type, makes it thus possible to include in the analysis other than metallic media. From the derivation for a wave at an interface between two media, one dielectric and one with a concentration of free electrons(do not has to be metal), he got the following equation:

$$(\varepsilon_s - \varepsilon_d)\omega^6 + \left[\left(\frac{\varepsilon_d}{\varepsilon_s} - 2\right)\omega_p^2 + \left(\frac{\varepsilon_d}{\varepsilon_s} - \frac{\varepsilon_s}{\varepsilon_d}\right)\beta^2 c^2\right]\omega^4 + \frac{1}{\varepsilon_s}\left(\omega_p^2 + 2\frac{\varepsilon_s}{\varepsilon_d}\beta^2 c^2\right)\omega_p^2\omega^2 - \frac{1}{\varepsilon_s\varepsilon_d}\omega_p^4\beta^2 c^2 = 0 \ . \tag{3.1}$$

ε_s is the permittivity of the layer with concentration of electrons(semiconductor). ε_d is the permittivity of dielectric. Equation (3.1) will lead us to three solutions of Surface Plasmons including two typical solutions and one novel solution exist only in semiconductor Surface Plasmons.

In this thesis, I do the derivation from classical method. The same process as shown

before was used to derive the SPPs at the metal/dielectric interface. Starting from the Maxwell's equation, we can get equations (2.20) and (2.21)

$$\frac{k_2}{k_1} = -\frac{\varepsilon_2}{\varepsilon_1}$$

$$\beta^2 + k_1^2 = \varepsilon_1 k_0^2$$

$$\beta^2 + k_2^2 = \varepsilon_2 k_0^2.$$

From the boundary condition $k_1 = k_2$ and $k_0 = \frac{\omega}{c}$, yield the following equation

$$(\varepsilon_1 - \varepsilon_2)[(\varepsilon_1 + \varepsilon_2)\beta^2 - \varepsilon_1\varepsilon_2(\frac{\omega}{c})^2]=0. \quad (3.2)$$

We can see that there are two parts of equation (3.2): $(\varepsilon_1 - \varepsilon_2)$ and $[(\varepsilon_1 + \varepsilon_2)\beta^2 - \varepsilon_1\varepsilon_2(\frac{\omega}{c})^2]$. Solve equation (3.2), let the second part equals zero

$$(\varepsilon_1 + \varepsilon_2)\beta^2 - \varepsilon_1\varepsilon_2(\frac{\omega}{c})^2 = 0. \quad (3.3)$$

Equation (3.3) yields the SPPs dispersion relation (2.22). In our case, ε_1 and ε_2 are the permittivity of semiconductor and dielectric.

Now we look into the Drude model and plasma frequency ω_p

$$\omega_p = \sqrt{\frac{Ne^2}{\varepsilon_0\varepsilon_s m^*}}. \quad (3.4)$$

ε_s represents the undoped permittivity of semiconductor which is equal to 1 for metal. Recall the Drude model $\varepsilon(\omega) = \varepsilon_\infty(1 - \frac{\omega_p^2}{\omega^2})$ without damping γ. Here for doped semiconductors, the infinite frequency permittivity ε_∞ becomes ε_s. The value of ε_s is known from the refractive index n of the undoped semiconductor: $\varepsilon_s = n^2$. Thus permittivity of semiconductor ε_1 now represented by Drude model for doped semiconductor

$$\varepsilon_1(\omega) = \varepsilon_s(1 - \frac{{\omega_p}^2}{\omega^2}). \quad (3.5)$$

Represent permittivity of dielectric by ε_d and taking equation (3.5) into (3.3) yields

$$\varepsilon_s\varepsilon_d\omega^4 - \left[(\varepsilon_s+\varepsilon_d)\beta^2c^2 + \varepsilon_s\varepsilon_d\omega_p^2\right]\omega^2 + \beta^2c^2\varepsilon_s\omega_p^2 = 0. \quad (3.6)$$

Solving equation (3.7), yields two solutions ω_1 and ω_2

$$\omega_{1,2}^2 = \frac{\omega_p^2}{2} + \frac{\varepsilon_s+\varepsilon_d}{2\varepsilon_s\varepsilon_d}\beta^2c^2 \pm \frac{1}{\varepsilon_s}\sqrt{\frac{\varepsilon_s^2\omega_p^4}{4} + \frac{\varepsilon_d-\varepsilon_s}{2\varepsilon_d}\varepsilon_s\omega_p^2\beta^2c^2 + \frac{(\varepsilon_s+\varepsilon_d)^2}{4\varepsilon_d^2}\beta^4c^4}. \quad (3.7)$$

In the classical derivation, $(\varepsilon_1 - \varepsilon_2)$ is ignored from equation (3.2) since the permittivity of metal is always smaller than the permittivity of dielectric. Take the Drude model (3.5) into $(\varepsilon_1 - \varepsilon_2) = 0$. Giving us

$$\varepsilon_s(1 - \frac{\omega_p^2}{\omega^2}) - \varepsilon_d = 0. \quad (3.8)$$

Finally yields

$$\omega_3^2 = \frac{\varepsilon_s\omega_p^2}{\varepsilon_s - \varepsilon_d}. \quad (3.9)$$

We can see that the new solution ω_3 for SPPs requires $\varepsilon_s > \varepsilon_d$, which explains why it cannot appear in the metal.

If we combine equation (3.7) and (3.9) by multiplying them to get the general equation for SPPs excited at a solid-state material plasma/dielectric interface we are looking for. It will give us equation (3.1) thus my result agreed well with Dr.Cada's work from the classical derivation. But the derivation in classical method is more easier and clearer to see the process and why the new solution is ignored.

Fig 3.2 below shows the two classical solutions ω_1 and ω_2 for the plasma frequency ω_p = 15eV. As it's supposed to, the plasmon's curve asymptotically approaches the value $\omega_p/\sqrt{2}$ when wavevector in x direction β approaches infinity. The straight line represents light in the air, and the upper branch when $\omega > \omega_p$ indicate the range that metal is transparent. We can see that Fig 3.2 is exactly the same with Fig 2.4 and indicate that equation (3.7) is applicable for the SPPs at metal/dielectric interface, obviously.

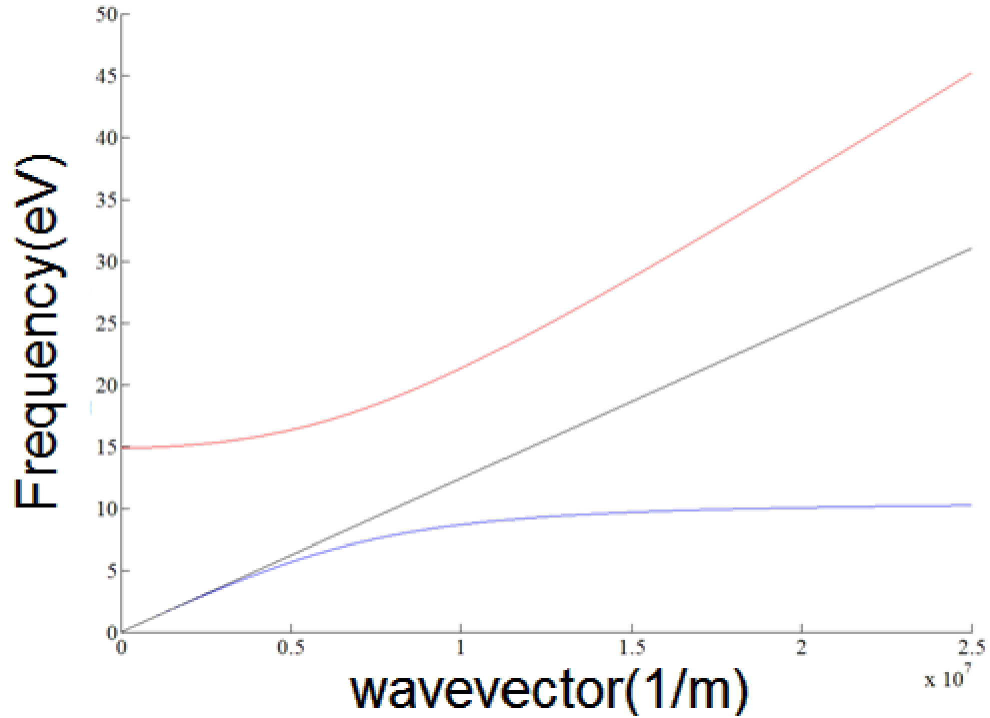

Figure 3.2 Classical dispersion curve for a surface plasmon at metal/air interface draws from equation (3.7). The straight line which is the light line also shown for reference.

Now we add the new solution ω_3 into the Fig 3.2. Fig 3.3 shows all the solutions including the new one for an Si/SiO_2 interface assuming an operating wavelength of 1.55µm (frequency, ω, is in eV, and the longitudinal propagation constant, β, is in 1/m).

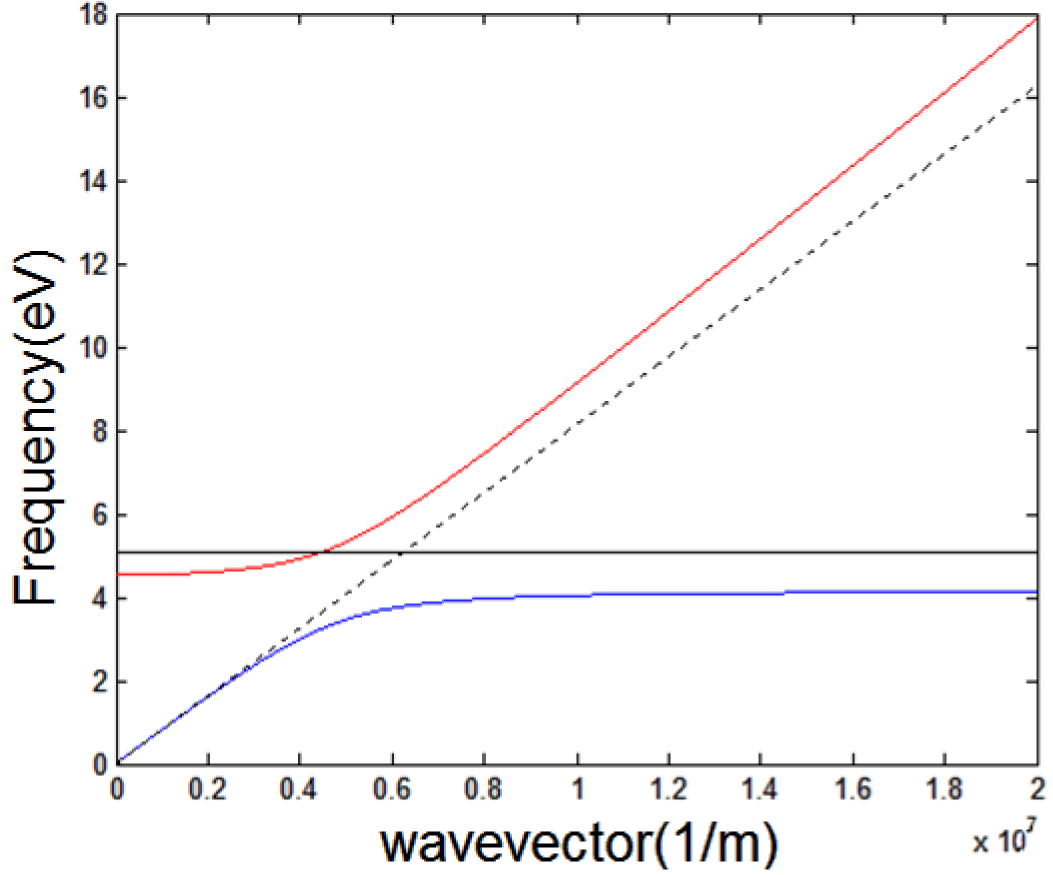

Figure 3.3 Dispersion characteristics of semiconductor/dielectric interface. New solution (solid line) and light (dash line) in dielectric are also shown.

We can see from Fig 3.3 that the new solution represents a "wave" with a zero group velocity but with any possible phase velocity. It crosses the light line, which indicates an existence of a new plasmonic-type wave.[19] The physical interpretation is not fully understood but it can be described like a standing wave which has the same characteristic in group and phase velocity.

Now we want to add damping and observe the effect of it on the new solution ω_3. Add damping factor γ into equation (3.5), yielding

$$\varepsilon_1(\omega) = \varepsilon_s(1 - \frac{\omega_p^2}{\omega^2 + i\omega\gamma}). \tag{3.10}$$

Taking equation (3.10) into $(\varepsilon_1 - \varepsilon_2) = 0$, (3.9) becomes

$$\omega_3 = -\frac{i\gamma}{2} \pm \sqrt{-\frac{\gamma^2}{4} + \frac{\varepsilon_s \omega_p^2}{\varepsilon_s - \varepsilon_d}}. \tag{3.11}$$

Eliminate the imaginary and negative part of frequency. Equation (3.11) yields

$$\omega_3^2 = \frac{\varepsilon_s \omega_p^2}{\varepsilon_s - \varepsilon_d} - \frac{\gamma^2}{4}. \quad (3.12)$$

From equation (3.12) we can see that the loss caused by damping reduces ω_3^2 by $\frac{\gamma^2}{4}$ compared to equation (3.9). The damping frequency γ which is equal to 1/τ here τ is the relaxation time. Losses from damping is ignored in most cases of metal because the condition ωτ >>1 is satisfied. While in a typical semiconductor, with $\tau \sim 10^{-13}$s at room temperature [10], it is safe to make the approximation ωτ >>1 at frequencies in the near-infrared. But we are looking into the heavily doped Silicon which has a free carrier concentration close to metal, and the relaxation time will be affected. We will discuss it in the following chapter.

3.3 Design and Data Selection

In this section, we are going to study the new solution of SPPs at semiconductor/dielectric interface numerically. We are also going to design a system to fulfill certain requirements. As we mentioned, the use of SPPs is considered to be a very promising way to close the gap between optical and electronic devices which is caused by the different size. We want the system to be comparable with electronic devices and also to work in the optical communication frequency range. We choose 1.55μm as the operating wavelength of the system because this is one of the three communication windows commonly used.

Choosing a proper material is crucial for the desired functionalities. From the previous derivation result equation (3.9) and (3.12), we can see that the new solution is related to plasma frequency $\omega_p = \sqrt{\frac{Ne^2}{\varepsilon_0 \varepsilon_s m^*}}$ and damping constant γ. As mentioned before, SPPs investigated at semiconductor/dielectric interface is in THz because it has a lower carrier density than metal. To excite SPPs in the optical frequency range, we have to use heavily doped semiconductors, and studies and data on the optical properties of this kind of material under heavily doped condition has to be mature. Also, the comparability between optical and electronic devices must be considered. Silicon come to mind. Silicon as a widely used material in current electronic and optical industry is less expensive than other material that could be used, is electronically comparable with circuits and has optical compatibility with fiber. It also takes lower losses than other materials. Due to the fabrication process of a two thin layer system in nano-scale, SiO_2 appears to be a good choice as the dielectric layer. Thus we are now investigating a heavily doped Silicon/SiO_2 structure with an operating wavelength equal to 1.55μm.

3.3.1 Properties of Heavily Doped Silicon

The doping technique for example ion implantation and laser annealing [26] makes it possible to dope Si with electrically active impurities to the level which significantly exceeds the thermal equilibrium solid solubility. The maximum peak carrier concentration is reported as $5*10^{21}$ cm^{-3}, which is close to the carrier density in metals. To do the numerical investigation of the new solution, the effect of heavily doping on Silicon to the properties of Silicon includes the effective mass and relaxation time will be studied.

3.3.2 Effective mass

Optical properties of free electrons in doped semiconductors have been investigated by many researchers[20], because they provide information concerning the conduction band. The pioneering work of Spitzer and Fan [21] indicated that the electron effective mass(m^*) can be determined by measuring the dielectric function. Since then, free electron absorption [22] and plasma reflectivity [23-25] experiments have been used to determine m^* and also to evaluate the doping homogeneity of semiconductor crystals.

The experimental data of free carrier effective mass for extremely heavily doped n-type silicon is measured in the infrared optical range (0.8 to 2.6μm) by Miyao et al. [27] and Howarth and Gilbert[28]. The theoretical approaches used by other researchers agreed to a large extent with the experiment data.

The heavy doping of impurities ($\geq 10^{21}$ cm^{-3}) without macroscopically extended defects is realized by high dose ion implantation and laser annealing.[27][28] Miyao provided two methods to measure the effective mass. First the values of m^* were determined from the relationship [21]

$$(\frac{1}{\lambda_{min}})^2 = \frac{e^2}{\pi c^2 (\varepsilon_s - 1) m^*} N \tag{3.13}$$

where ε_s is the dielectric constant of non-doped crystal, c is the light velocity and e is the electron charge. The same effective masses of $0.28m_0$(m_0 is the electron rest mass) were obtained in the carrier concentration region below 10^{21} cm^{-3}. When m^* exceeds 10^{21} cm^{-3}, for samples of different doping levels — i.e. $3*10^{21}cm^{-3}$ and $5*10^{21}cm^{-3}$ — the effective mass is 0.45 m_0 and $0.55m_0$. m^* increases with the increase in carrier concentration and the values are the same for different dopants, such as P and As used by Miyao's experiment. The second method starts by analyzing the transmittance (T) by the two layer model. The free carrier absorption in the infrared region is measured and the Drude model is used for analysis. This analysis also measured the value of relaxation time, which will be discussed in the next section. Fig 3.4 shows the relation between the effective mass and relaxation time with carrier concentration. We can see the values of m^* derived from two methods (dark and light circles) are shown and the same relation between m^* and N was obtained by using different methods.

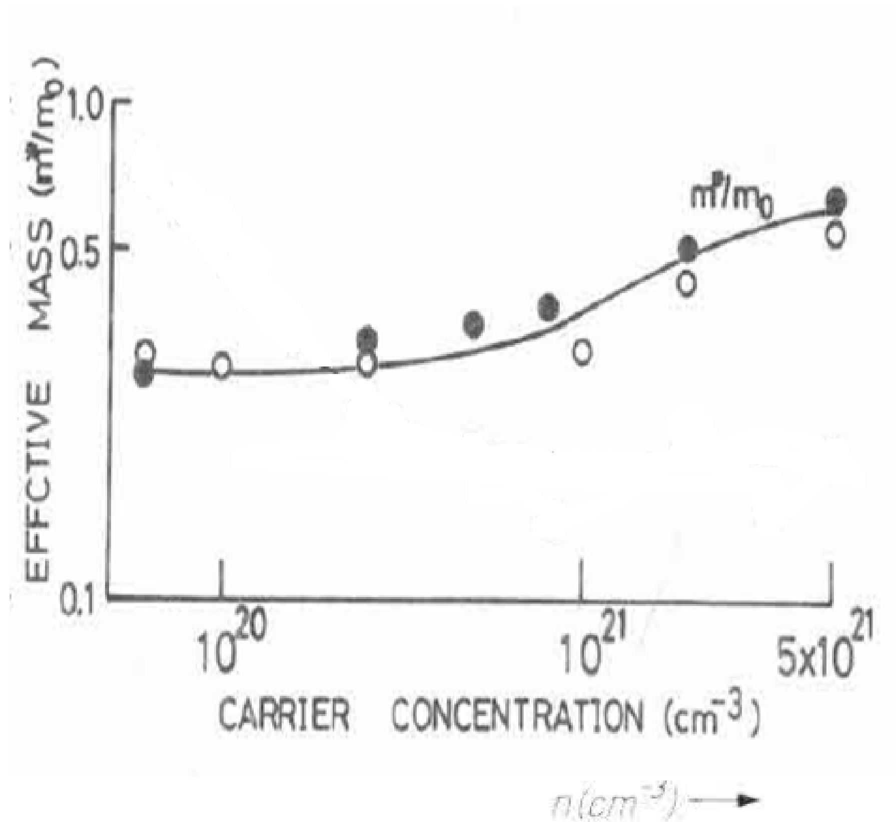

Figure 3.4 Carrier concentration dependence of free electron effective mass (m^*) and carrier relaxation time (τ).[27]

The other groups of researchers tried to provide the theoretical approach after a short period of time.[29][30] Slaoui and Siffert considered two models based on Durde's theory. The first model assumes an almost uniform doped layer, while in the second model, the active carrier concentration after implantation and annealing is considered to vary exponentially with depth. We chose the second model — the exponentially distributed (inhomogeneous doping) model — because there is more available data on it, which makes it easier to make comparisons with the approach and results of the other papers on the topic.

In the case of inhomogeneous doping, the following equation describes the propagation of the light in the medium,

$$\frac{d^2E_y(x)}{dx^2} + \left(\frac{\omega}{c}\right)^2 \varepsilon^*(\omega, x)E_y(x) = 0 \qquad (3.14)$$

where E_y is the intensity of the electric field. Use following expression to express the carrier concentration profile after implantation and laser annealing.

$$N(x) = N_0 + N_{max}\exp[-\alpha(x-d)^2] \quad for \;\; x \geq d, \qquad (3.15a)$$

$$N(x) = N_0 + N_{max}\exp[-\beta(x-d)^2] \quad for \;\; x < d, \qquad (3.15b)$$

where N_0 is the doping of the substrate, N_{max} is the maximum concentration of dopants and d the depth location of this maximum from the surface. α and β are adjustable parameters. The solution of equation (3.14) for this model yields the following value of the reflection coefficient[31]:

$$R(\omega) = \frac{[V(0)-1]^2+(\frac{cW(0)}{\omega})^2}{[V(0)+1]^2+(\frac{cW(0)}{\omega})^2}. \qquad (3.16)$$

We can see that the two unknown quantities V and W at the surface (x=0) decide the coefficient R(ω). V and W determined from the differential equations

$$\frac{dW}{dx} + W^2 - (\frac{\omega}{c})^2[V^2 - \varepsilon_r(\omega, x)] = 0 \qquad (3.17a)$$

$$\frac{dV}{dx} + 2WV - \left(\frac{\omega}{c}\right)^2 \varepsilon_i(\omega, x) = 0. \qquad (3.17b)$$

To use the certain numerical resolution method of these equations to calculate V and W along the doping profile: one starts from the substrate where the concentration N is constant and step by step one progresses towards the surface[31].

Then first assumes a dopant profile characterized by the α, β, d, N_{max} parameters and supposes a relaxation time τ_0 (for $N>10^{21}$ cm^{-3}) and an effective mass m_e^*. Calculate the V(0) and W(0) quantities for each wavelength and infer R(ω). Finally revise the value of τ_0 and m_e^* to get the lowest difference between the experimental and theoretical spectra for each free carrier density. After the steps above, Fig 3.5 is given which include the experimental data from [27] and [28] while the dashed line is the theoretical approach calculated from the band structure data [29]. And the light circle shows the inhomogeneous profile while the dark circle represents the homogeneous profile, here we only look into the inhomogeneous case as mentioned before.

Now we come to another approach, which is considered more accurate and we chose as data source for our final numerical calculation. In Miyao's paper, the increase of effective mass with the increase of carrier density is explained as the result of entrance into a new valley of electrons which have over flown the conventional valley. Yet Driel[29] claimed that the filling of new band theory from Miyao is not the main factor in the increase of effective mass. He indicated that the electron mass behavior, which is observed experimentally, occurs primarily because of the increasing warping of the ellipsoidal constant energy surfaces with increasing Fermi energy.[29]

Therefore, we made a theoretical calculation of the high density optical effective mass based on the known band structure and empirical pseudopotential method[32]. They give effective mass for electrons at both 300K and 3000K in Fig 3.6. We are now only interested in the electron mass at room temperature (Fig 3.6 solid curve). In Fig 3.6, the measurements of the mass of electrons from Miyao et al. [27] and Howarth and Gilbert [28] at room temperature is also shown for comparison. We can see that the approaching curve matches the experiment data well, thus we will take the values of heavily doped electron effective mass of silicon from the solid curve in Fig 3.6.

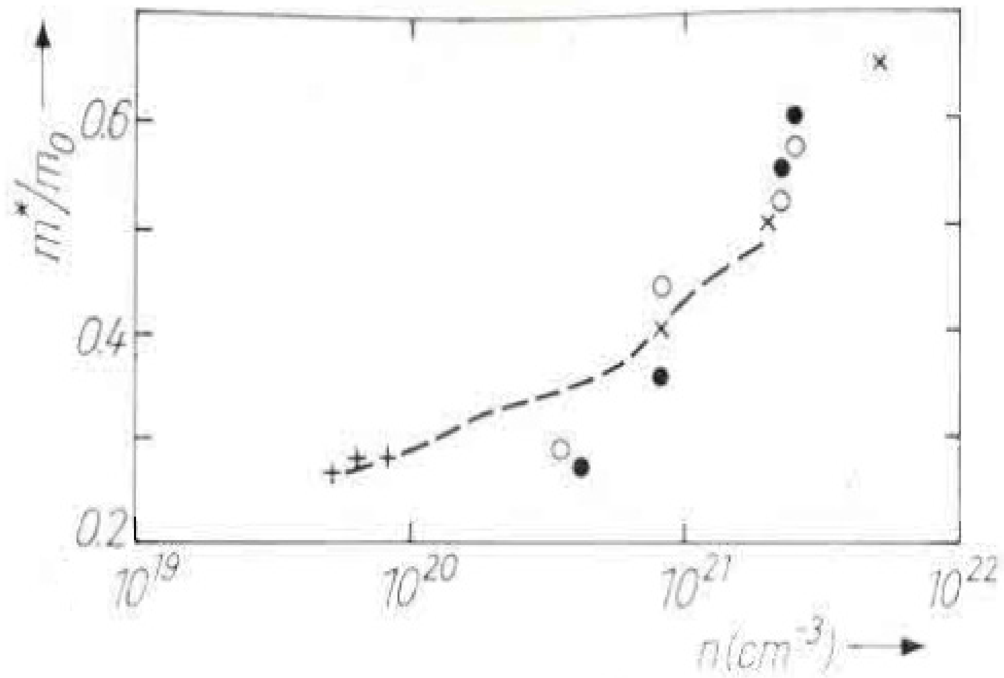

Figure 3.5 Effective mass of free carriers as a function of carrier concentration. The dashed line gives the effective mass of electrons calculated from the band structure data [29]; +[28],×[27], ● homogeneous profile, ○ inhomogeneous profile.[30]

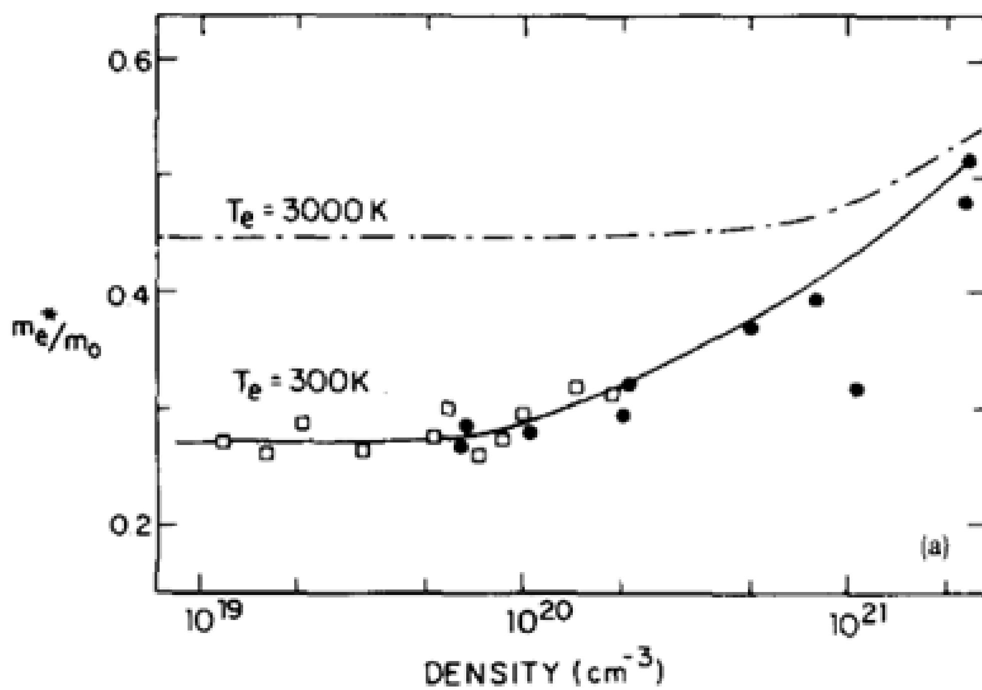

Figure 3.6 Density dependence of the electron effective mass of electrons for T = 300K (solid curve) and T = 3000K (dash-dot curve). The data points indicated are those of Miyao et.al.[27] and Howarth and Gilbert[28].[29]

3.3.3 Relaxation Time

In this section, the relaxation time of heavily doped Silicon will be discussed. As we mentioned, in a typical semiconductor, relaxation time τ is around 10^{-13}s at room temperature [10]. In the former section, the process of deciding the relation between the free carrier density and effective mass also included the analysis of relaxation time τ based on the Drude model.[27][30] The relation between relaxation time τ and free carrier density N is shown in Fig 3.7 and Fig 3.8 from Miyao and A.Slaoui.

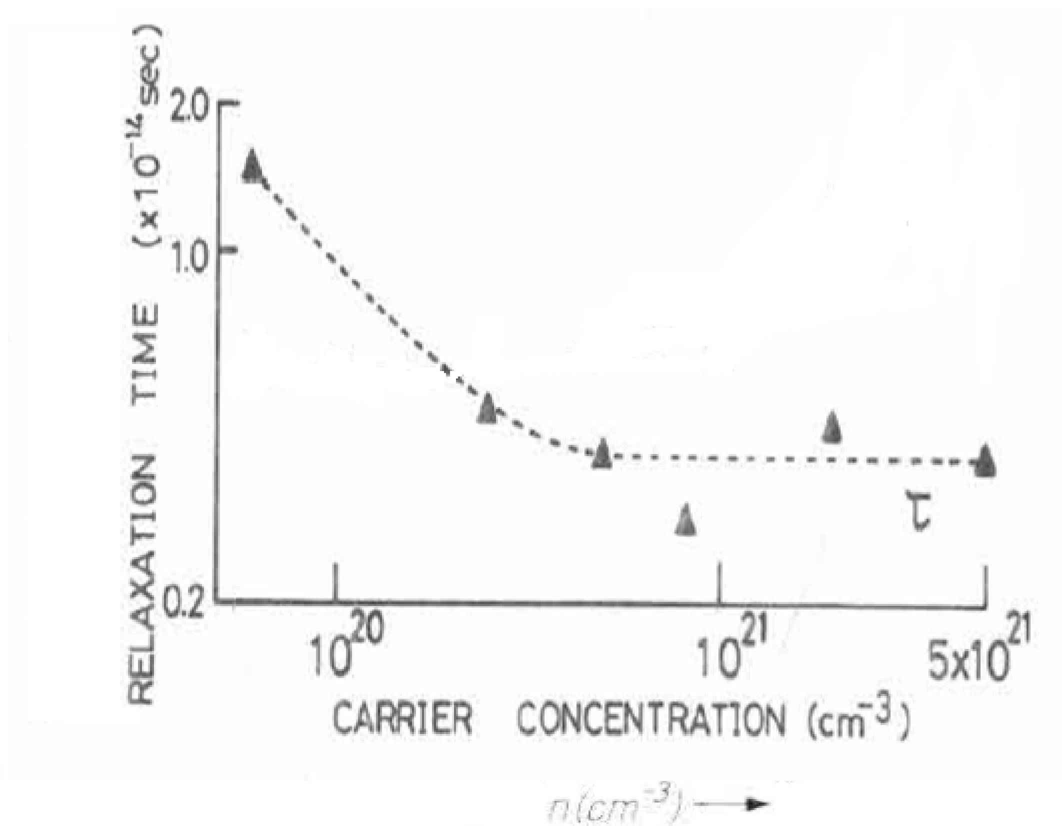

Figure 3.7 Carrier concentration dependence of carrier relaxation time (τ).[27]

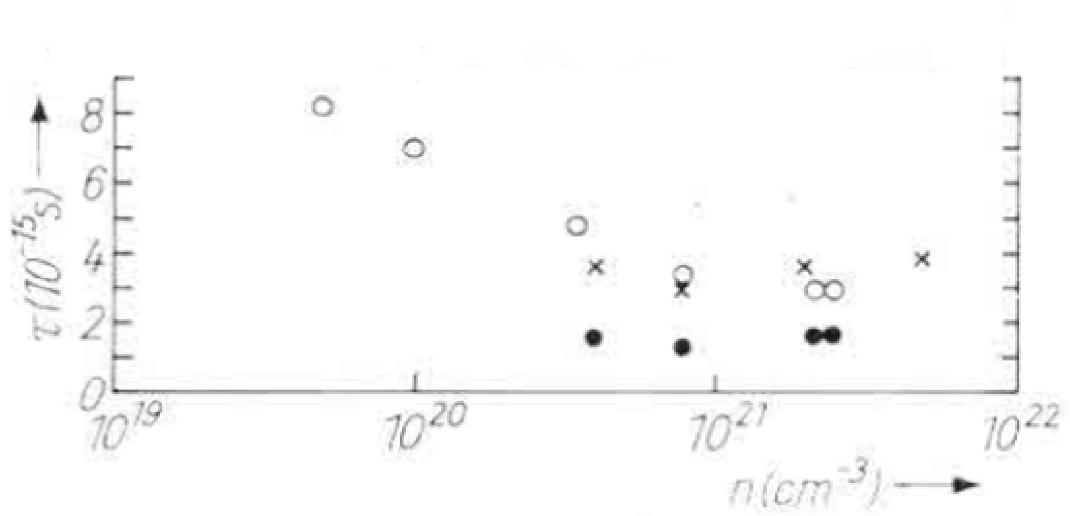

Figure 3.8 Relaxation time of free carriers as a function of carrier concentration. ×[27], ● homogeneous profile, ○ inhomogeneous profile.[30]

We can see that the measured value from two groups of researchers agree well. The relaxation time decreases with higher carrier concentration and saturates at $\tau = 3*10^{-15}$s, for $N_e > 10^{21}$ cm^{-3}. Here the main competing mechanisms are scattering by acoustic vibrations of the lattice and scattering by ionized impurity ions. The relaxation time is saturated when carrier density exceeds $10^{21}cm^{-3}$ and while the first process is independent of carrier density N, the second depends on it. Hence, we can say that the scattering by acoustic vibration is the primary process in the heavily doped n-type Silicon and the value of damping constant γ is easily chosen as $1/3*10^{-15}$.

CHAPTER 4

RESULTS and DISCUSSIONS

In this chapter, we are going to do the calculation of the value of ω_3 excited together with the SPPs at Silicon/SiO_2 (Fig. 4.1) interface based on section 3.4. We will also try to achieve the goal of exciting the new plasmon mode ω_3 at operating wavelength 1.55μm. At the end, an error analysis of the design will be made to deal with errors.

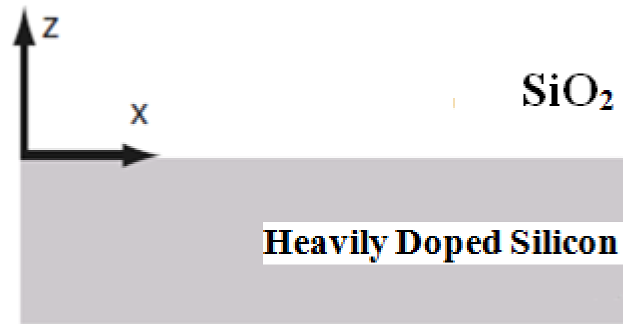

Figure 4.1 Structure used to excite SPPs

Recall the equation (3.9) $\omega_3^2 = \frac{\varepsilon_s \omega_p^2}{\varepsilon_s - \varepsilon_d}$ and (3.12) $\omega_3^2 = \frac{\varepsilon_s \omega_p^2}{\varepsilon_s - \varepsilon_d} - \frac{\gamma^2}{4}$ which are the formulas to exclude and include the loss from damping correspondingly. First we will take a calculation for both equations (3.9) and (3.12) to compare the difference. Now we are going to list the values of the constant variables and variables introduced by the equations above in the following paragraph.

At room temperature, the permittivity of undoped Silicon ε_s and Silicon Dioxide (SiO_2) is equal to 12.094 [33] and 2.3339 [34] at 1.55μm. For plasma frequency $\omega_p =$

$\sqrt{\frac{Ne^2}{\varepsilon_0 \varepsilon_s m^*}}$, e is the charge of the electron equals to 1.6^2*10^{-19}C, and $\varepsilon_0 = 8.85*10^{-12}$ F·m^{-1} is the permittivity of free-space. The damping constant $\gamma = 1/\tau$ where $\tau = 3 * 10^{-15}$s when the free carrier density is larger than 10^{27}m^{-1} [27][30]. N is the electron density which is the first variable; the second variable m^* is the value of electron effective mass in heavily doped Silicon which is taken from Fig 3.6.

4.1 The Effect of Damping on ω_3

To observe how the damping affects ω_3, we are going to take a sample value to calculate equation (3.9) and (3.12) to see the effect of damping to ω_3. Fig 4.2 shows the plot of SPPs excited at heavily doped Silicon/SiO_2 interface when the electron density of doped Silicon is equal to $2.5*10^{27}$ m^{-3}, and the value of ω_3 is given in the graph drawn by Matlab. The effective mass of electrons m^* at this carrier density is interpolated from the value Fig 3.6, which is equal to $0.517m_0$.

From Fig 4.2(a) and (b), we can see that the value of ω_3 with and without damping is equal to 0.8187eV and 0.8260eV. ω_3 is reduced 0.0073eV by loss from damping which is less than one per cent. Thus we can conclude that damping is not affecting the system a lot and can be ignored. This is because the semiconductor with such a high level carrier density will have a plasma frequency close to metal. Thus $\omega_p * \tau \gg 1$ and damping can be ignored. In order to get a more precise value, we will include damping in the following calculations.

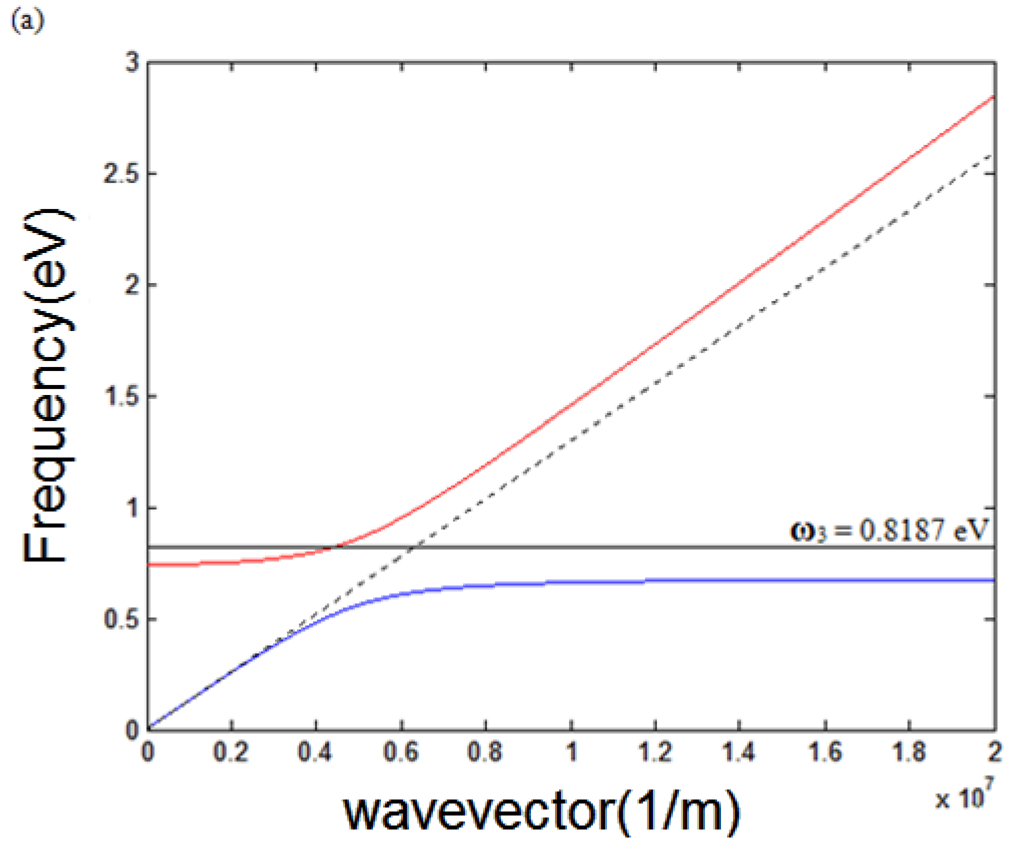

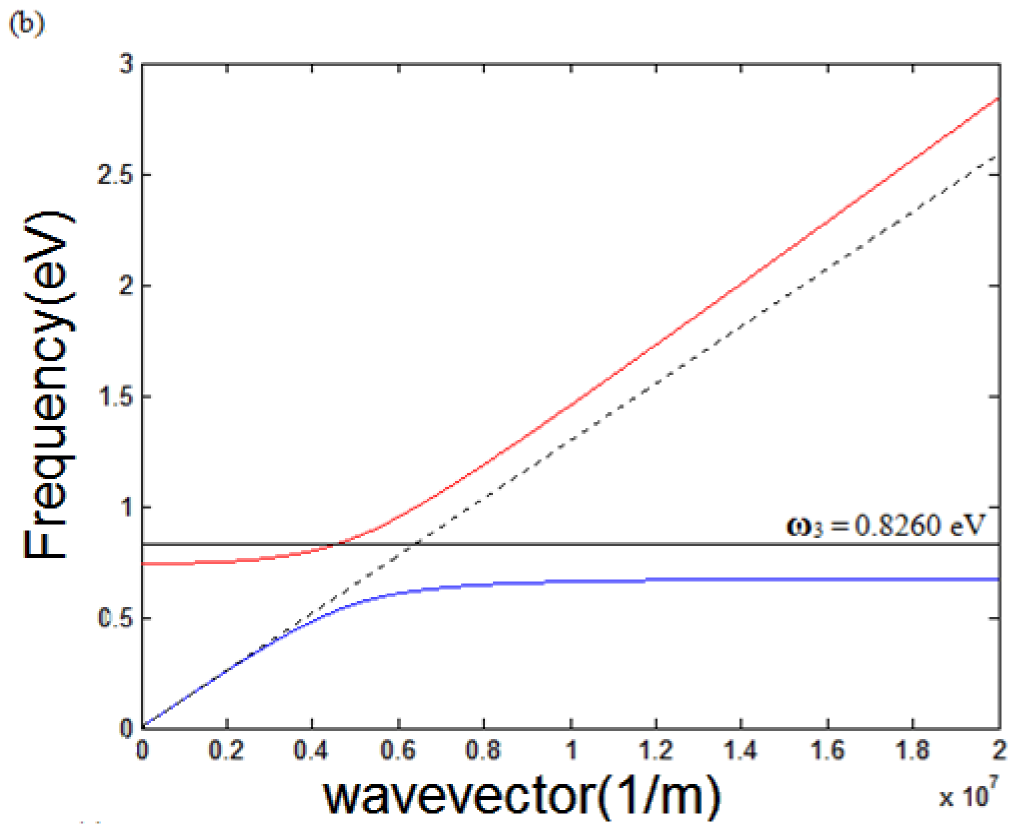

Figure 4.2 SPPs dispersion characteristics at Si/SiO_2 interface with electron density of Si equal to $2.5*10^{27}$ m^{-3}, (a) ω_3 ignore loss from damping equation (3.9) and (b) ω_3 contain loss from damping equation (3.12)

4.2 System Design and Analysis of the Result

Again, our goal is to excite ω_3 by coupling a light source with 1.55µm wavelength (in air) with electron plasma in heavily doped Silicon. In the figures shown below, the y-axis which represents frequency is in the unit electron-Volt(eV), while 1.55µm wavelength in air corresponds to 0.8 eV. The SPPs dispersion relations and the value of ω_3 for four sample carrier densities of $1*10^{27}m^{-3}$, $1.5*10^{27}m^{-3}$, $2*10^{27}m^{-3}$ and $3*10^{-3}m^{-3}$ are shown in Fig 4.3 to 4.6.

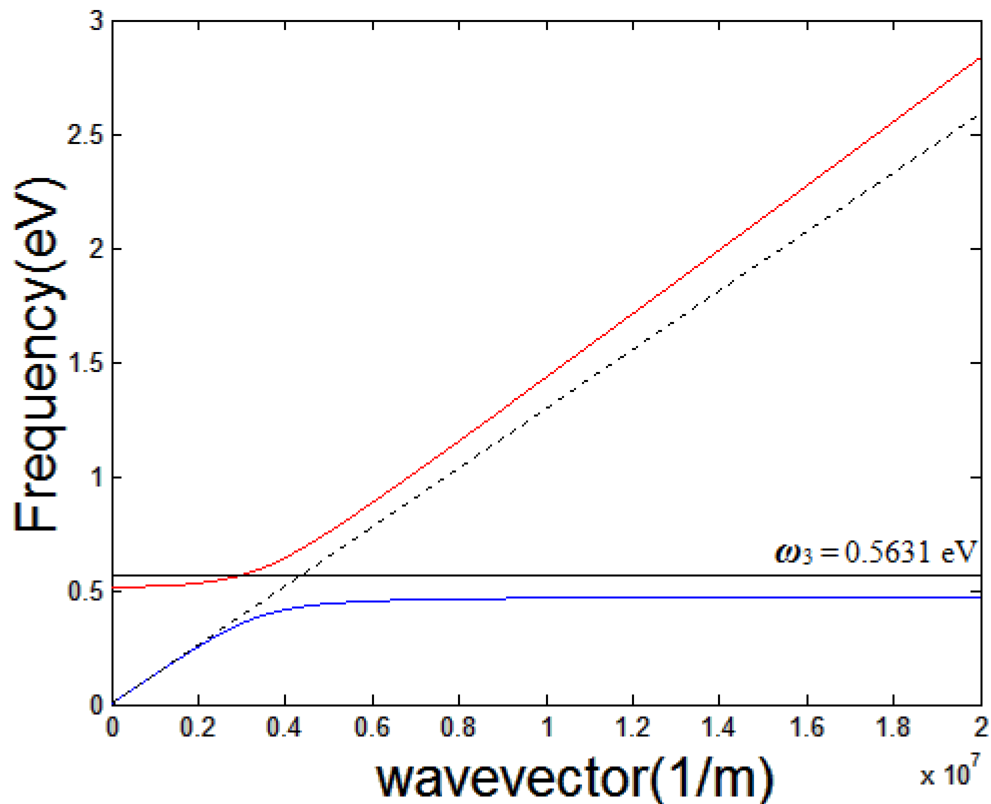

Figure 4.3 SPPs dispersion characteristics at Si/SiO_2 interface with electron density of Si equal to $1*10^{27}$ m^{-3} and ω_3 = 0.5631 eV.

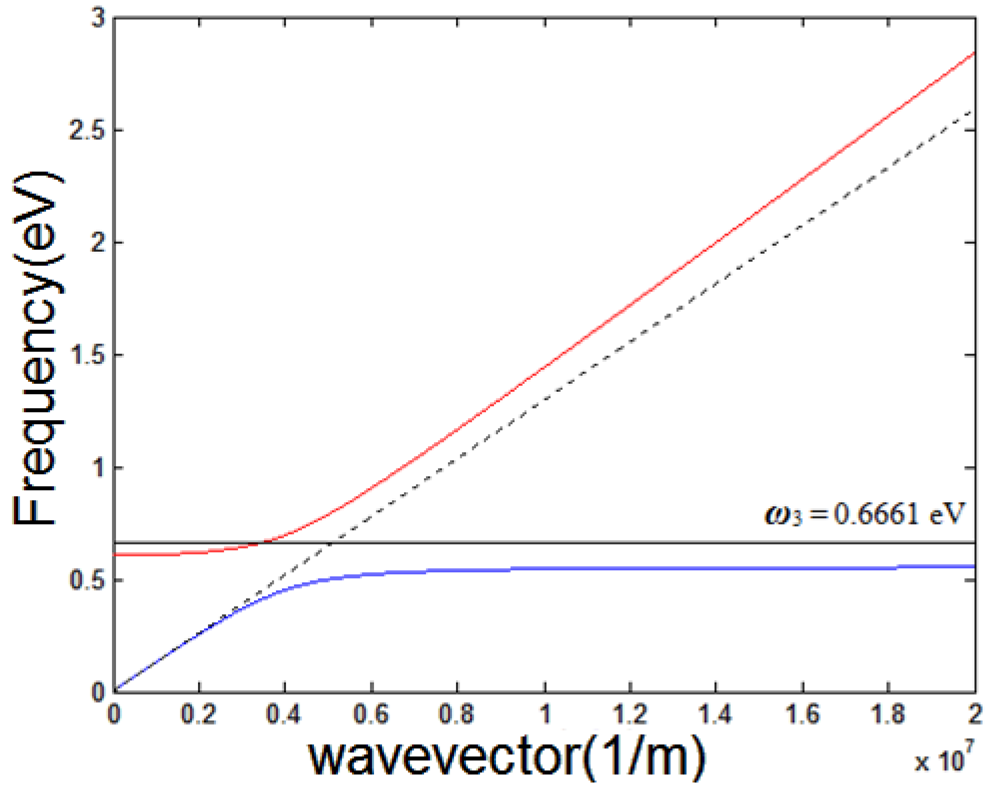

Figure 4.4 SPPs dispersion characteristics at Si/SiO_2 interface with electron density of Si equal to $1.5*10^{27}$ m^{-3} and ω_3 = 0.6661 eV.

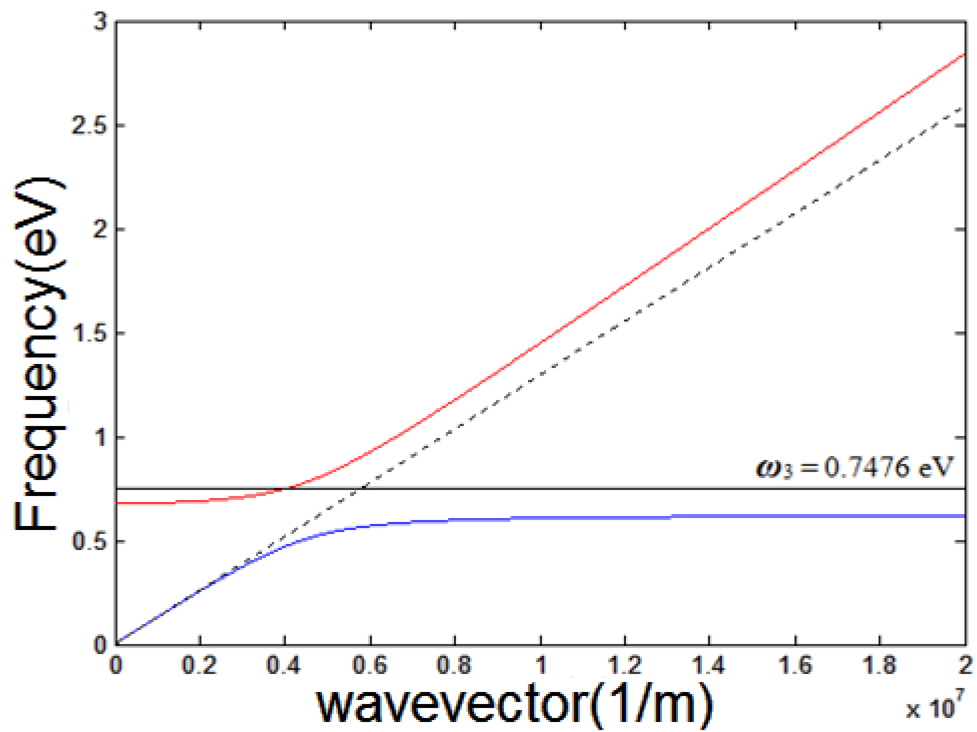

Figure 4.5 SPPs dispersion characteristics at Si/SiO_2 interface with electron density of

Si equal to $2*10^{27}$ m^{-3} and ω_3 = 0.7476 eV.

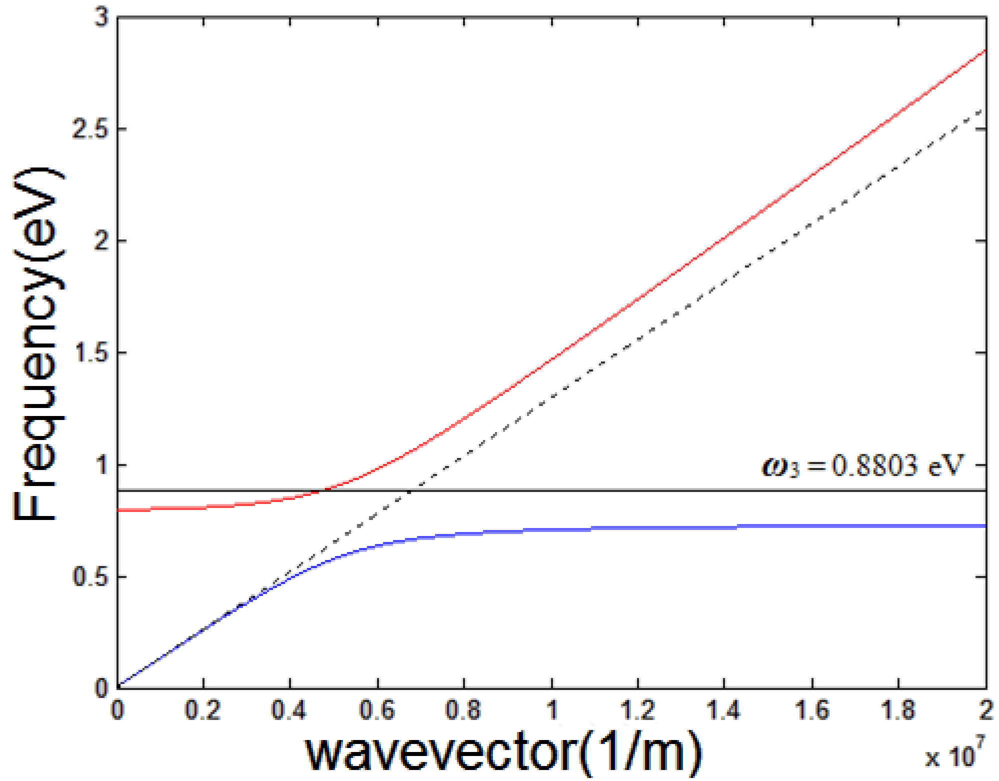

Figure 4.6 SPPs dispersion characteristics on Si/SiO_2 interface with electron density of Si equal to $3*10^{27}$ m^{-3} and ω_3 = 0.8803 eV.

From Fig 4.3 to 4.6 and Fig 4.2(b), we can see that the value of ω_3 increased with the increase of carrier density. ω_3 at sample electron densities are shown in Table 1 with the corresponding wavelengths.

Table 1 Value of ω_3 for sample free electron densities and corresponding wavelength

Electron density N (m^{-3})	**Effective mass m^*/m_0**	**ω_3 (eV)**	**Wavelength of ω_3 (μm)**
$1*10^{27}$	0.4287	0.5631	2.202
$1.5*10^{27}$	0.4644	0.6661	1.861
$2*10^{27}$	0.4942	0.7476	1.658
$2.5*10^{27}$	0.5170	0.8187	1.514
$3*10^{27}$	0.5379	0.8803	1.408

By these sample values of ω_3, we can predict that the 1.55μm (0.8 eV) will appear in the range between $2*10^{27}m^{-3}$ to $3*10^{27}m^{-3}$. Inputting the data of free electron densities and effective mass of free electrons of Silicon into Minitab yields the regression equation between N and m^*. The plot of the equation and samples are shown in Fig 4.7 as follow:

Regression Analysis: m^* versus N

The regression equation is
$m^* = 0.380 + 0.0542 N$

8 cases used, 12 cases contain missing values

Predictor	Coef	SE Coef	T	P
Constant	0.380040	0.007662	49.60	0.000
N	0.054200	0.003612	15.01	0.001

S = 0.00571057 R-Sq = 98.7% R-Sq(adj) = 98.2%

Analysis of Variance

Source	DF	SS	MS	F	P
Regression	1	0.0073441	0.0073441	225.21	0.001
Residual Error	3	0.0000978	0.0000326		
Total	4	0.0074419			

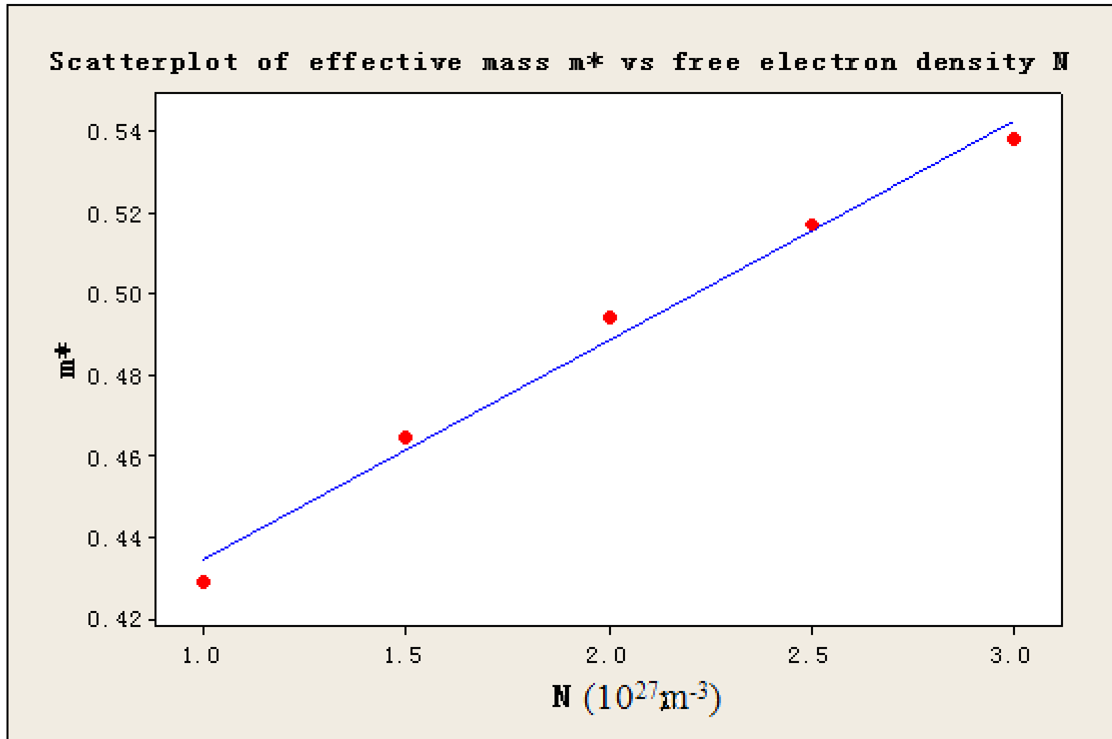

Figure 4.7 Plot of the regression equation and sample points

It yields the regression equation

$$m^* = 0.380 + 0.0542\,N. \tag{4.1}$$

We can see that the correlation coefficient R-Sq = 98.7%. In a qualitative sense, R-Sq near 1 means a good fit of the data to the regression line and R-Sq near zero means a poor fit. Thus equation (4.1) describes the relation between N and m^* well in this range. It needs to be recognized that the number of samples used to find the regression equation is fairly small; thus this approach still needs to be checked by interpolating from Fig 3.6.

Taking the regression equation (4.1) into the Matlab program, by setting $\omega_3 = 0.8$eV, we can get the corresponding free electron density, which is $2.35*10^{27}m^{-3}$. By interpolating from Fig 3.6, effective mass $m^* = 0.5080m_0$ at free carrier density $2.35*10^{27}m^{-3}$ while $m^* = 0.50737m_0$ from regression equation (4.1). Taking both values into calculation and drawing the dispersion curve, we can get Fig 4.8 below. We can see that the ω_3 is very close in both cases, which are 0.8009 eV and 0.8004 eV.

It is close enough to our goal (0.8eV => 1.55μm) as a reference data for the future work. Hence we conclude that at the free electron density of Silicon equal to $2.35*10^{27}m^{-3}$, the ω_3 of wavelength 1.55μm can be excited by an impinging light with 0.8 eV.

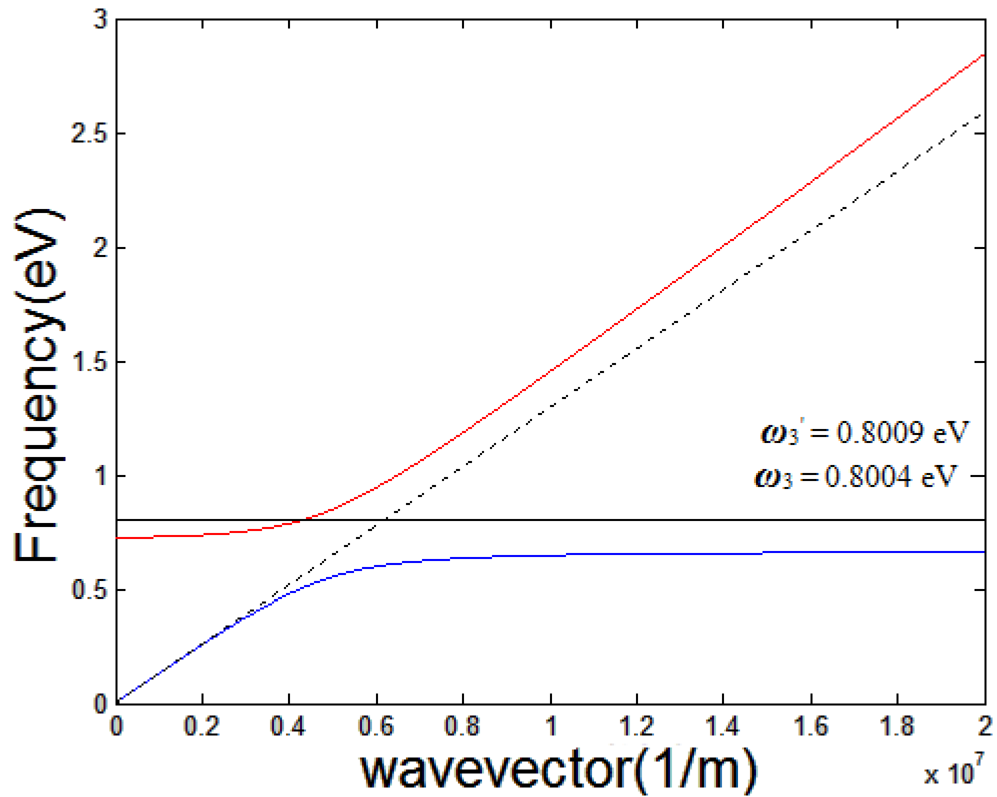

Figure 4.8 SPPs dispersion relation at free electron density $2.35*10^{27}m^{-3}$, ω_3 and ω_3' are calculated for $m^* = 0.5080m_0$ and $m^* = 0.50737m_0$ which are interpolated from Fig.3.6 and from regression equation (4.1).

4.3 Error Analysis

By using a step-by-step approach to get to our final results, errors could have been introduced by taking the values of effective mass m^* and relaxation time τ. Since the value of τ is a constant in the region we are interested in, while the value of m^* is interpolated from theoretical approach Fig 3.6, we can predict that effective mass is the cause of errors.

The errors of effective mass come from two parts, one is the experimental error in the published data, and the other one is from the interpolation. The first issue is unavoidable because although the error introduced by an experiment is not given in the paper, it could easily be 5-10%. For example, in Fig 3.6, the experimental data of effective mass from Miyao [27] at electron density $N = 1.03*10^{21}m^{-3}$ is $0.316m_0$, while from the theoretical approach, effective mass is equal to $0.434m_0$. There is a difference equal to $0.118m_0$ between the experimental data and theoretical value, which will cause a 0.1023eV difference in ω_3. But this is an unusual point even in the experimental data; most of the data are fitted well with the theoretical approach and within a 5 per cent difference between them.

To test the tolerance of the system to error which may have been induced by effective mass, we vary the value of it by 5 per cent and observe the difference introduced by this change. The comparison between the original value of ω_3 and the value after reducing effective mass by 5 per cent are shown in Table 2.

Table 2 Values of original ω_3 and ω_3' which were calculated from reducing the effective mass by 5 per cent

Electron Density N ($10^{27}m^{-3}$)	**ω_3 (eV)**	**ω_3' (eV)**	**Percentage of Change**
1	0.5631	0.5783	2.70%

Electron Density N ($10^{27}m^{-3}$)	**ω_3 (eV)**	**ω_3' (eV)**	**Percentage of Change**
1.5	0.6661	0.6839	2.67%
2	0.7476	0.7675	1.99%
2.5	0.8187	0.8403	2.64%
3	0.8803	0.9035	2.64%
2.35	0.8004	0.8216	2.65%

From table 2 we can tell that the 5 per cent change in effective mass which represents the error may introduce 2.6 per cent change in the result of ω_3. The system's tolerance of error introduced from effective mass is acceptable.

CHAPTER 5

CONCLUSION and FUTURE WORK

5.1 Conclusion and Contribution

In the thesis, we investigated the Surface Plasmon Polaritons at heavily doped semiconductor/dielectric interface. Compared to the traditional metal/dielectric structure, SPPs excited at semiconductor/dielectric interface can be controlled by modifying the free carrier density of semiconductor. Current research on Surface Plasmons at semiconductors/dielectric interface are in millimeter wavelength (terahertz frequencies) and have been believed not to support plasmons at optical frequency.

Theoretical and initial numerical studies were conducted on plasmonic interactions at a semiconductor/dielectric interface. A derivation was performed for a wave at an interface between two media, one dielectric and one with a concentration of free electrons. Based on the classical theoretical treatment, we describe the layer with free electrons by the Drude-model and found a new solution that does not exist at metal/dielectric interfaces.

Silicon/SiO_2 has been chosen as our prototype structure for several reasons. By investigating the optical properties of heavily doped Silicon, we proved through numerical calculations that ω_3 can be excited under 1.55μm operating wavelength when the electron density equal to $2.35*10^{27}m^{-3}$. Error analysis has been taken into account to deal with the errors introduced during the step by step approach

5.2 Future work

As can be seen from Fig 3.3, the new solution ω_3 represents a wave with a zero group velocity but with any possible phase velocity. The physical meaning of it is not fully understood and an experiment based on our numerical research needs to be conducted. Also, light source in visible and near infrared region can excite ω_3 and the same step has to be taken to approach the certain result. Also, other kinds of semiconductors can be used to replace Silicon like AlGaAs etc., which have different optical properties and may provide us with other features. Finally, the imaginary part of the dielectric equation from the Drude-model needs to be included in the future to include the losses. Other models describing plasma may give us a better approach of the dielectric function of semiconductors.

BIBLIOGRAPHY

[1] Wood, R.W. (1902). On a remarkable case of uneven distribution of light in a diffraction grating spectrum. Proc. Phys. Soc. London, 18:269–275

[2] Fano, U. (1941). The theory of anomalous diffraction gratings and of quasi-stationary waves on metallic surfaces (Sommerfeld's waves). J. Opt. Soc. Am., 31:213–222.

[3] Ritchie, R. H. (June 1957). "Plasma Losses by Fast Electrons in Thin Films". Physical Review 106 (5): 874–881.

[4] Ritchie, R. H., Arakawa, E. T., Cowan, J. J., and Hamm, R. N. (1968). Surface-plasmon resonance effect in grating diffraction. Phys. Rev. Lett., 21(22):1530–1533.

[5] Kretschmann, E. and Raether, H. (1968). Radiative decay of non-radiative surface plasmons excited by light. Z. Naturforschung, 23A:2135–2136.

[6] Otto, A. (1968). Excitation of nonradiative surface plasma waves in silver by the method of frustrated total reflection. Z. Physik, 216:398–410.

[7] Stefan Alexander Maier (2007). PLASMONICS: FUNDAMENTALS AND APPLICATIONS. New York: Springer-Verlag.

[8] Reuven Gordon. Surface Plasmon Nanophotonics: A Tutorial. IEEE NANOTECHNOLOGY MAGAZINE, September 2008:12-18.

[9] R. Merlin, "Radiationless electromagnetic interference: Evanescent-field lenses and perfect focusing," Science, vol. 317, no. 5840, pp. 927–929, 17 Aug. 2007.

[10] M. Fox, Optical Properties of Solids. Oxford University Press 2010.

[11] Wikipedia:The Free Encyclopedia. [online]
Available: http://en.wikipedia.org/wiki/Helmholtz_equation.

[12] Yariv, Amnon (1997). *Optical Electronics in Modern Communications*. Oxford Univeristy Press, Oxford, UK, fifth edition edition.

[13] H. Raether, *Surface plasmons on smooth and rough surfaces and on gratings*, Springer-Verlag, Berlin, (1986)

[14] Lukas Novotny and Bert Hecht (2006), "Principles of Nano-Optics", Cambridge university press.

[15]Devaux, Eloise, Ebbesen, ThomasW.,Weeber, Jean-Claude, and Dereux, Alain (2003). Launching and decoupling surface plasmons viamicro-gratings. *Appl. Phys. Lett.*, 83(24):4936–4938.

[16] Jose A.Sanchez-Gil, Jaime Gomez Rivas (2006), "Thermal switching of the scattering coefficients of terahertz surface plasmon polaritons impinging on a finite array of subwavelength grooves on semiconductor sufaces", Phys. Rev B 73,205410.

[17] Kyungjun Song and Pinaki Mazumder(Jul 2011), "Dynamic Terahertz Spoof Surface Plasmon-Polariton Switch Based on Resonance and Absorption", IEEE Transactions on electron devices, VOL. 58, No.7.

[18] T.M.Rumke et al.,"Local and anisotropic excitation of surface plasmon polaritons by semiconductor nanowires", OPTICS EXPRESS-5013, Vol. 16, No.7 Mar 2008.

[19] Michael Cada, Jaromir Pistora(2008), "Optical Plasmons in Semiconductors", refereed proceedings, ISMOT, Prague, P.P 23-29, June 2011.(Invited plenary talk)

[20] R.A. Abram, G.J.Ress & B.L.H. Wilson, Adv.Phys. 27, 799(1978).

[21] W.G.Spitzer & H.Y.Fan, Phys.Rev. 106,882(1957).

[22] W.G.Spitzer & J.M. Whelan, Phys, Rev. 114,59 (1959).

[23] E.E. Gardner, W.Kappallo & C.R. Gordon, Appl Phys Lett. 9, 432(1966).

[24] L.E.Howarth & J.F.Gilbert,J.Appl.Phys. 34, 236(1963).

[25] V.K. Subashiev, G.B.Dubrovskii & A.A. Kukharskii, Sov.Phys.Solid State 6,830 (1964).

[26] Proc.Laser-Solid Interactions and Laser Processing(1978); (Edited by S.D.Ferris, H.J.Leamy & J.M.Poate). American Inst.Phys.,N.Y.(1979).

[27] M.Miyao, T.Motooka,N.Tatsuaki, and T.Tokuyama, Solid State Commun.37,605 (1981).

[28] L.E.Howarth and J.F.Gilbert, J.Appl.Phys.34, 236(1963).

[29] H.M. van Driel, Optical effective mass of high density carriers in silicon, Appl.Phys.Lett. 44(6), 15 March 1984.

[30] A.Slaoui and P.Siffert, Determination of the electron effective mass and relaxation time in heavily doped silicon. Phys. Stat.Sol.(a) 89,617 (1985).

[31] A.Slaoui, 3e Cycle thesis, Louis Pasteur University, Strasbourg (1984).

[32] M.L. Cohen and V.Heine, in Solid State Physics, edited by H.Ehrenreich, F.Seitz, and D.Turnbull (Academic,New York, 1970), Vol.24, p.38.

[33] Marvin J.Weber, Handbook of Optical Materials. CRC Press (2003).

[34] Gorachand Ghosh. Dispersion-equation coefficients for the refrative index and birefringence of calcite and quartz crystals. Opt.Commun. 163, 95-102(1999).